NLR Mutations Suppressing Immune Hybrid Incompatibility and Their Effects on Disease Resistance[1][OPEN]

Kostadin E. Atanasov,[a] Changxin Liu,[a] Alexander Erban,[b] Joachim Kopka,[b] Jane E. Parker,[c] and Rubén Alcázar[a,2]

[a]Department of Biology, Healthcare and Environment, Section of Plant Physiology, Faculty of Pharmacy and Food Sciences, University of Barcelona, 08028 Barcelona, Spain

[b]Max Planck Institute for Molecular Plant Physiology, 14476 Potsdam, Germany

[c]Department of Plant-Microbe Interactions, Max Planck Institute for Plant Breeding Research, 50829 Cologne, Germany

ORCID IDs: 0000-0002-5538-895X (K.E.A.) (K.E.A.); 0000-0003-0723-7812 (C.L.); 0000-0003-1794-588X (A.E.) (A.E.); 0000-0001-9675-4883 (J.K.); 0000-0002-4700-6480 (J.E.P.); 0000-0002-3567-7586 (R.A.)

Genetic divergence between populations can lead to reproductive isolation. Hybrid incompatibilities (HI) represent intermediate points along a continuum toward speciation. In plants, genetic variation in disease resistance (*R*) genes underlies several cases of HI. The progeny of a cross between Arabidopsis (*Arabidopsis thaliana*) accessions Landsberg *erecta* (L*er*, Poland) and Kashmir2 (Kas2, central Asia) exhibits immune-related HI. This incompatibility is due to a genetic interaction between a cluster of eight *TNL (TOLL/INTERLEUKIN1 RECEPTOR-NUCLEOTIDE BINDING-LEU RICH REPEAT) RPP1 (RECOGNITION OF PERONOSPORA PARASITICA1)-like* genes (*R1–R8*) from L*er* and central Asian alleles of a *Strubbelig*-family receptor-like kinase (*SRF3*) from Kas2. In characterizing mutants altered in L*er*/Kas2 HI, we mapped multiple mutations to the *RPP1*-like L*er* locus. Analysis of these *suppressor of Ler/Kas2 incompatibility* (*sulki*) mutants reveals complex, additive and epistatic interactions underlying *RPP1-like* L*er* locus activity. The effects of these mutations were measured on basal defense, global gene expression, primary metabolism, and disease resistance to a local *Hyaloperonospora arabidopsidis* isolate (*Hpa* Gw) collected from Gorzów (Gw), where the Landsberg accession originated. Gene expression sectors and metabolic hallmarks identified for HI are both dependent and independent of *RPP1-like* L*er* members. We establish that mutations suppressing immune-related L*er*/Kas2 HI do not compromise resistance to *Hpa* Gw. QTL mapping analysis of *Hpa* Gw resistance point to *RPP7* as the causal locus. This work provides insight into the complex genetic architecture of the *RPP1-like* L*er* locus and immune-related HI in Arabidopsis and into the contributions of *RPP1-like* genes to HI and defense.

Hybrid vigor is a common phenomenon in plants. Genetic differentiation between individuals of the same species at specific loci can also lead to a dramatic reduction of hybrid fitness in the F1 or later generations, due to negative epistasis. Certain interacting alleles are not deleterious in their respective backgrounds, but they can become lethal when combined in the same hybrid genome. Such negative genetic interactions might constitute an early stage of species isolation (Coyne, 1992; Coyne and Orr, 2004). Plant hybrid necrosis or hybrid weakness has been documented in crops and model species (Bomblies and Weigel, 2007). In the last decade, identification of genetic determinants of some hybrid incompatibilities (HIs) revealed that immune gene variability could underlie this phenomenon. Immune-related incompatible hybrids are temperature dependent and exhibit reduced growth, deregulated cell death, and sterility (Bomblies et al., 2007; Alcázar et al., 2009; Jeuken et al., 2009; Yamamoto et al., 2010; Chen et al., 2014). The metabolic costs of maintaining a constitutively active immune system might contribute to reduced fitness. In many cases, mapping of causal genes identified at least one polymorphic *Nucleotide-binding/Leu-rich-repeat* (*NLR*) locus encoding intracellular pathogen recognition (NLR) receptors (Alcázar et al., 2012; Chae et al., 2014). *NLR*-interacting loci include other disease *Resistance* (*R*) genes or genes with diverse functions (Bomblies and Weigel, 2007; Alcázar et al., 2009; Yamamoto et al., 2010; Chae et al., 2014). In Arabidopsis (*Arabidopsis thaliana*), the *DANGEROUS MIX2* (*DM2*) locus mapping to a

[1]This work was supported by the Ramón y Cajal Program (RYC-2011-07847) of the Ministerio de Ciencia e Innovación (Spain), by grants from the Programa Estatal de Fomento de la Investigación Científica y Técnica de Excelencia (Ministerio de Economía y Competitividad, Spain; BFU2013-41337-P and BFU2017-87742-R) cofinanced with FEDER (Fondo Europeo de Desarrollo Regional), and by a Marie Curie Career Integration grant (DISEASENVIRON, PCIG10-GA-2011-303568) of the European Union. K.E.A., C.L., and R.A. are members of the Grup de Recerca Consolidat 2017 SGR-604 of the Generalitat de Catalunya. K.E.A. acknowledges support from the Subprograma Estatal de Formación del Ministerio de Economía y Competitividad (BES-2014-068041). R.A. and J.E.P. acknowledge support of Deutsche Forschungsgemeinschaft (CRC 680) for part of this work.

[2]Address correspondence to ralcazar@ub.edu.

The author responsible for distribution of materials integral to the findings presented in this article in accordance with the policy described in the Instructions for Authors (www.plantphysiol.org) is: Rubén Alcázar (ralcazar@ub.edu).

K.E.A., J.K., J.E.P., and R.A. designed the research; K.E.A. and R.A. performed research with contributions from C.L. and A.E.; K.E.A., A.E., J.K., J.E.P., and R.A. analyzed data; R.A. conceived the project and wrote the article with contributions from all authors.

[OPEN]Articles can be viewed without a subscription.

www.plantphysiol.org/cgi/doi/10.1104/pp.18.00462

polymorphic *RPP1* (*RECOGNITION OF PERONOSPORA PARASITICA1*)-*like* gene cluster underlies at least five documented cases of immune-related HIs between accessions Uk-1 (*DM2*, *RPP1-like*)/Uk-3 (*DANGEROUS MIX1*, *SUPPRESSOR OF SALICYLIC ACID INSENSITIVE4*; Bomblies et al., 2007), Landsberg *erecta* (L*er*) (DM2, *RPP1-like*)/Kas2 (*STRUBBELIG RECEPTOR FAMILY3*; Alcázar et al., 2009), Bla-1 (*DM2*, *RPP1-like*)/Hh-0 (*DANGEROUS MIX3*, prolyl aminopeptidase *At3g61540*), Dog-4 (*DM2*, *RPP1-like*)/ICE163 (*DANGEROUS MIX5*), and TueWa1-2 (*RPP1-like*)/ICE163 (*DANGEROUS MIX4*, overlapping with *RPP8*; Chae et al., 2014). Therefore, the *RPP1-like* locus is a hotspot for temperature-dependent immune-related HI in Arabidopsis (Alcázar et al., 2009; Chae et al., 2014; Stuttmann et al., 2016).

Immune-related HIs have also been reported in rice (*Oryza sativa*), lettuce (*Lactuca sativa*), tomato (*Solanum lycopersicum*), the genus *Capsella*, and other species. An interspecific hybrid weakness in rice involves two dominant loci and three genes (Chen et al., 2014). One locus (*HYBRID WEAKNESS I1*) contains two *LRR RECEPTOR-LIKE KINASE* genes, both required for incompatibility with the *HYBRID WEAKNESS I2* locus, which maps to a *SUBTILISIN-LIKE PROTEASE* gene (Chen et al., 2014). Also in rice, a two-way recessive interaction causing hybrid breakdown involves the *CASEIN KINASE I* gene and an *NLR* cluster (Yamamoto et al., 2010). In lettuce, temperature-dependent hybrid necrosis in an interspecific cross involves two loci, one of them mapping to *RPM1 INTERACTING PROTEIN4*, encoding an acylated plasma membrane-associated protein that is a negative regulator of basal antimicrobial defense targeted by different *Pseudomonas syringae* effectors (Jeuken et al., 2009; Khan et al., 2016). In tomato, HI was observed in an interspecific cross involving allelic variants at *Rcr3* and *Cf2* loci, the latter conferring resistance to the fungus *Cladosporium fulvum* (Krüger et al., 2002). In the genus *Capsella*, HI has been described between *Capsella grandiflora* and *Capsella rubella* involving a two-way epistatic interaction between *NPR1* and *RPP5* loci (Sicard et al., 2015). The Dobzhansky-Muller model on genetic incompatibilities is agnostic on whether causal genes diverge into incompatible alleles by drift or selection (Coyne and Orr, 2004). The frequency of immune receptor genes underlying HI is likely a consequence of their rapid evolution in response to pathogen infection pressure (Chae et al., 2014).

The majority of plant disease *R* genes encode NLR proteins. These are classified into two main groups: TNLs (TIR-NLRs) and CNLs (CC-NLRs), based on the presence of a Toll/IL-1 receptor (TIR) or a coiled-coil CC domain at their N terminus (Sukarta et al., 2016). *R* genes often reside in clusters and exhibit high polymorphism and copy number variation, through illegitimate recombination, duplication, and gene conversion events (Bakker et al., 2006; Hurwitz et al., 2010; McHale et al., 2012; Muñoz-Amatriaín et al., 2013). Indeed, together with *RECEPTOR-LIKE KINASE* genes, *NLRs* exhibit signatures of rapid expansion and diversification (Cao et al., 2011; Xu et al., 2011). The *RPP1-like* locus contains a variable number of *TNL* genes in different Arabidopsis accessions, from two in Col-0 to four in Ws2 (Botella et al., 1998), five to six in Zdr1 and Est1 (Goritschnig et al., 2016) and eight in L*er*, Uk-1, and Bla-1 (Alcázar et al., 2009; Chae et al., 2014). *RPP* genes recognize the obligate biotrophic oomycete pathogen, *Hyaloperonospora arabidopsidis* (*Hpa*, formerly *Peronospora parasitica*), which causes downy mildew disease (Botella et al., 1998; Coates and Beynon, 2010). As a naturally coevolving host-pathogen system, different *Hpa* isolates have been identified that elicit accession-specific resistance responses due to the recognition of different avirulence gene products/effectors (*Arabidopsis thaliana* Recognized [ATR]) or effector variants. The *RPP1* resistance locus in Ws2 and Nd1 contains *RPP1* genes that exhibit partially overlapping recognition of *Hpa* isolates (Botella et al., 1998; Rehmany et al., 2005). Using an F2 mapping population derived from a cross between *Hpa* isolates Emoy2 (avirulent) and Maks9 (virulent), ATR1^{NdWsB} was found to be recognized by RPP1-NdA (Rehmany et al., 2005). Genetic variation at *ATR1* conditions *Hpa* recognition by different *RPP1* genes, e.g. *RPP1*-WsB, *RPP1*-NdA, *RPP1*-EstA, and *RPP1*-ZdrA (Rehmany et al., 2005; Sohn et al., 2007; Goritschnig et al., 2016). RPP1 receptors likely also perceive other *ATR* gene products (Botella et al., 1998; Rehmany et al., 2005). An intriguing question is whether *RPP1* genes involved in immune-related HIs provide disease resistance to locally adapted *Hpa* isolates or their activities in pathogen resistance and incompatibility can be separated.

Here, we determine the contribution of different *RPP1-like* genes to L*er*/Kas2 HI and resistance to a local *Hpa* isolate collected in Gorzów Wielkopolski (Poland), where Landsberg was collected in 1939. In this population, 30% of genetically differentiated Gorzów (Gw) individuals contain a conserved *RPP1-like* L*er* haplotype. This derived haplotype increased in frequency and has been maintained locally for many generations (Alcázar et al., 2014). Through ethyl methanesulfonate (EMS) mutagenesis, we identify multiple *suppressors of Ler/Kas2 incompatibility* (*sulki*) mutants, which map to *RPP1-like* L*er R3* and *R8* genes. Generation of CRISPR/Cas9 *RPP1-like* L*er R2*, *R3*, *R4*, and *R8* loss-of-function mutants in a L*er*/Kas2 near-isogenic line (NIL) background reveals that additive and epistatic interactions between *RPP1-like* gene members contribute to immune-related HI. Global gene expression and metabolite profiling of L*er*/Kas2 incompatible hybrids and *sulki* suppressors identify metabolic and expression hallmarks for immune-related HIs, which are *RPP1-like R8* dependent or independent. Through QTL mapping, we find that resistance to the local *Hpa* isolate from Gorzów (denoted here *Hpa* Gw) in L*er* is not mediated by genes at the *RPP1-like* locus but maps to a region containing the previously defined *RPP7* CNL *Resistance* gene (McDowell et al., 2000). Resistance conferred by *RPP7* to *Hpa* Gw is genetically independent of

salicylic acid (SA) and *EDS1*. Because certain *RPP1-like* proteins recognize allelic variants of the *Hpa* ATR1 effector, we tested whether RPP1-like L*er* proteins could induce host cell death, reflecting a hypersensitive response (HR) when transiently expressed with *Hpa* Gw ATR1 in tobacco (*Nicotiana tabacum*). Coexpression of *RPP1-like* L*er* R2, R3, R4, or R8 protein with *Hpa* Gw ATR1δ51 does not trigger cell death in tobacco. Our results show that the *RPP1-like*-incompatible haplotype does not provide disease resistance to a local *Hpa* Gw isolate. We provide evidence for complex genetic interactions underlying the *RPP1-like* L*er* locus HI with Kas2. Our results also help differentiate *RPP1-like* gene actions in incompatibility and defense.

RESULTS

Identification of *RPP1-like* L*er* Suppressors of L*er*/Kas2 Incompatibility

An incompatible L*er*/Kas2 NIL that contains a L*er* introgression spanning the *RPP1-like* locus in an otherwise Kas2 genetic background (Alcázar et al., 2009) was used for the isolation of *suppressor of Ler/Kas2 incompatibility* (*sulki*) mutants. Mutagenized L*er*/Kas2 NIL plants were generated by treating L*er*/Kas2 NIL seeds with EMS, and 25,000 M1 individuals were propagated in 200 pools. Approximately 1,000 M2 generation plants from each pool were grown to identify suppressors of HI at 14°C to 16°C. Twenty dominant *sulki* mutants were isolated, which suppressed dwarfism at 14°C to 16°C, indicative of a loss or amelioration of L*er*/Kas2 HI. The different *sulki* mutants were backcrossed at least five times with the parental L*er*/Kas2 NIL. The genomes of *sulki* BC_5F_1 and L*er*/Kas2 NIL were then sequenced by next-generation sequencing, and unique SNPs were identified for each mutant compared with the L*er*/Kas2 NIL.

DNA sequence analysis identified eleven *sulki* mutants carrying single mutations within the *RPP1-like* L*er* locus, which were further confirmed by SANGER sequencing (Fig. 1A). Ten intragenic mutations (*sulki1-1* to *sulki1-10*) were dominant, mapping to different domains of *RPP1-like* L*er R8*, and fully suppressed both dwarfism and cell death at low temperature (14°C–16°C; Figs. 1A and 2; Supplemental Fig. S1; Supplemental Table S1). *RPP1-like* L*er R8* is a homolog of *DANGEROUS MIX 2h* (*DM2h*) in Arabidopsis accessions Uk-1 and Bla-1 (Chae et al., 2014). In Col-0, it is homologous to *At3g44670* (Alcázar et al., 2014), although with a high level of polymorphism especially in the LRR domain (Chae et al., 2014). A recessive mutation (*sulki2-1*) mapped to the TIR domain of *RPP1-like* L*er R3* (T78I), which partially suppressed dwarfism and cell death (Fig. 2; Supplemental Fig. S1; Supplemental Table S1). In all cases, except for one 8-nucleotide deletion (*sulki1-7*), only G/C to A/T transition mutations were observed, as expected for mutations generated by EMS treatment (Fig. 1A).

Distribution of *sulki* Mutations within TIR, NB, and LRR Domains

In *RPP1-like* L*er R8*, five and three suppressor mutations were found in the NB and LRR domains, respectively (Fig. 1B), consistent with the importance of these domains in TNL function (Meyers et al., 2003). Amino acid changes were found within the conserved RNBS-C (P428S, *sulki1-2*) and GLPL (P466L, *sulki1-3*) motifs. Two additional amino acid substitutions (G500E in *sulki1-5* and G509A in *sulki1-6*) and one stop codon (W484*, *sulki1-4*) were in a stretch of 40 amino acids that connects GLPL and RNBS-D motifs. The presence of three close mutations leading to the same suppressive phenotype suggests that the GLPL-to-RNBS-D region is crucial for *RPP1-like* L*er* R8 function. Three additional amino acid changes were found in the LRR domain of *RPP1-like* L*er R8*, in the junction between LRR2 and LRR3 (S758F, *sulki1-8*), within LRR5 (R821H, *sulki1-9*) and LRR8 (G877E, *sulki1-10*) motifs. A small 8-nucleotide deletion was identified in the splice donor site of *sulki1-7*, preceding the LRR exon. In the TIR domain of *RPP1-like* L*er R8*, one G202E nonsynonymous substitution was detected between TIR3 and TIR4 in *sulki1-1* (Fig. 1B). Most suppressive nonsynonymous substitutions were found in invariant or highly conserved NLR residues, except for Gly-509, which appears to be specific to *RPP1-like* L*er* R8 homologs *At3g44670* $^{\text{Col-0}}$ and *DM2h* $^{\text{Bla-1}}$ (Supplemental Fig. S2).

All together, we identified multiple independent mutations within the NB or LRR domains of *RPP1-like* L*er R8* and single mutations in the TIR domains of *RPP1-like* L*er R8* and *R3* genes suppressing L*er*/Kas2 NIL immune-related HI. These data strongly reinforce previous studies identifying *RPP1-like* L*er R3* and *R8* as genes contributing to L*er*/Kas2 HI (Alcázar et al., 2014; Stuttmann et al., 2016). We concluded that single point mutations within the *RPP1-like* locus are sufficient for full (*sulki1*, *RPP1-like* L*er R8*) or partial (*sulki2*, *RPP1-like* L*er R3*) suppression of L*er*/Kas2 HIs.

Expression of SA-Responsive and Oxidative Stress Marker Genes in *sulki1* and *sulki2*

L*er*/Kas2 HI is associated with constitutive activation of TNL receptor-triggered defense programs, including high expression of *PR1*, *EDS1*, *GST1*, and *RPP1-like* L*er R3* at 14°C to 16°C (Alcázar et al., 2009, 2014). We analyzed transcripts of these and other *RPP1-like* L*er* genes (*R2*, *R4*, and *R8*) to determine the defense status of *sulki1* and *sulki2*. Expression of *PR1*, *EDS1*, and *GST1* was much lower in *sulki1* and *sulki2-1* mutants compared to the L*er*/Kas2 NIL but similar or slightly lower than L*er* or Kas2 (Fig. 3). These results suggest that constitutive activation of defenses in the L*er*/Kas2 NIL at 14°C to 16°C is suppressed in *sulki1* and *sulki2*. The expression of *RPP1-like* L*er R3* and *R8* was also significantly lower in *sulki1* and *sulki2* than in L*er*/Kas2 NIL (Fig. 3). We hypothesized that SA, which accumulates in L*er*/Kas2 NIL (Alcázar et al.,

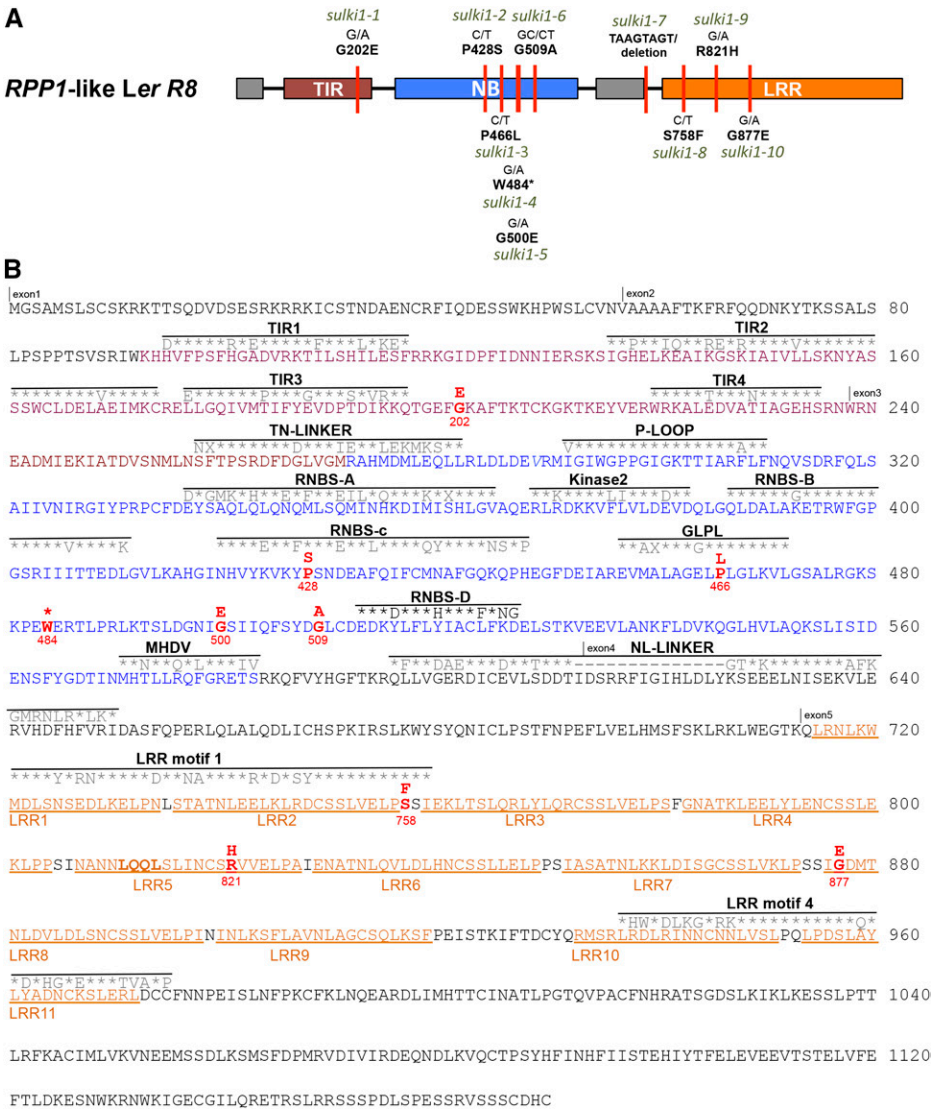

Figure 1. *sulki1* mutations mapping to *RPP1-like R8* L*er*. A, Schematic representation of nonsynonymous substitutions identified in *sulki1* mutants. Exon/intron organization and Toll-IL receptor (TIR), nucleotide binding (NB), and Leu-rich repeat (LRR) domains are shown. B, Detailed representation of *RPP1-like R8* L*er* amino acid sequence, conserved motifs (Meyers et al., 2003), and position of *sulki1* mutations.

2009), causes up-regulation of some *RPP1-like* genes. Indeed, we found that *RPP1-like* L*er R3* and *R8*, but not *R2* or *R4*, expression was induced in L*er* by SA or benzo (1,2,3) thiadiazole-7-carbothioic acid *S*-methyl ester application at 8 to 24 h (Supplemental Fig. S3). Therefore, we concluded that there is SA-positive feedback regulation of *RPP1-like* L*er* genes *R3* and *R8* involved in immune-related HI.

Allelism and Complementation Tests of *sulki1 and sulki2* Mutants

To confirm that the causal mutations in *sulki1* map to *RPP1-like* L*er R8*, we performed allelism tests with *RPP1-like* L*er R8* loss-of-function mutants generated by CRISPR/Cas9 in the L*er*/Kas2 NIL background (referred to as Cas9-*r8*; Supplemental Fig. S4). Cas9-*r8* mutants that contained early stop codons in the TIR domain of *RPP1-like* L*er R8* suppressed dwarfism and cell death at 14°C to 16°C in a dominant manner, consistent with the involvement of *RPP1-like* L*er R8* in the incompatibility with Kas2 (Fig. 4A; Supplemental Fig. S5; Supplemental Table S1). To confirm that *sulki1* mutations were allelic to Cas9-*r8*, homozygous *sulki1* and Cas9-*r8-1* (after removal of the *Cas9* transgene) were crossed, and F2 populations were obtained by selfing. The F2 populations were screened for the occurrence of incompatible phenotypes at 14°C to 16°C (Supplemental Table S1). The absence of segregation for

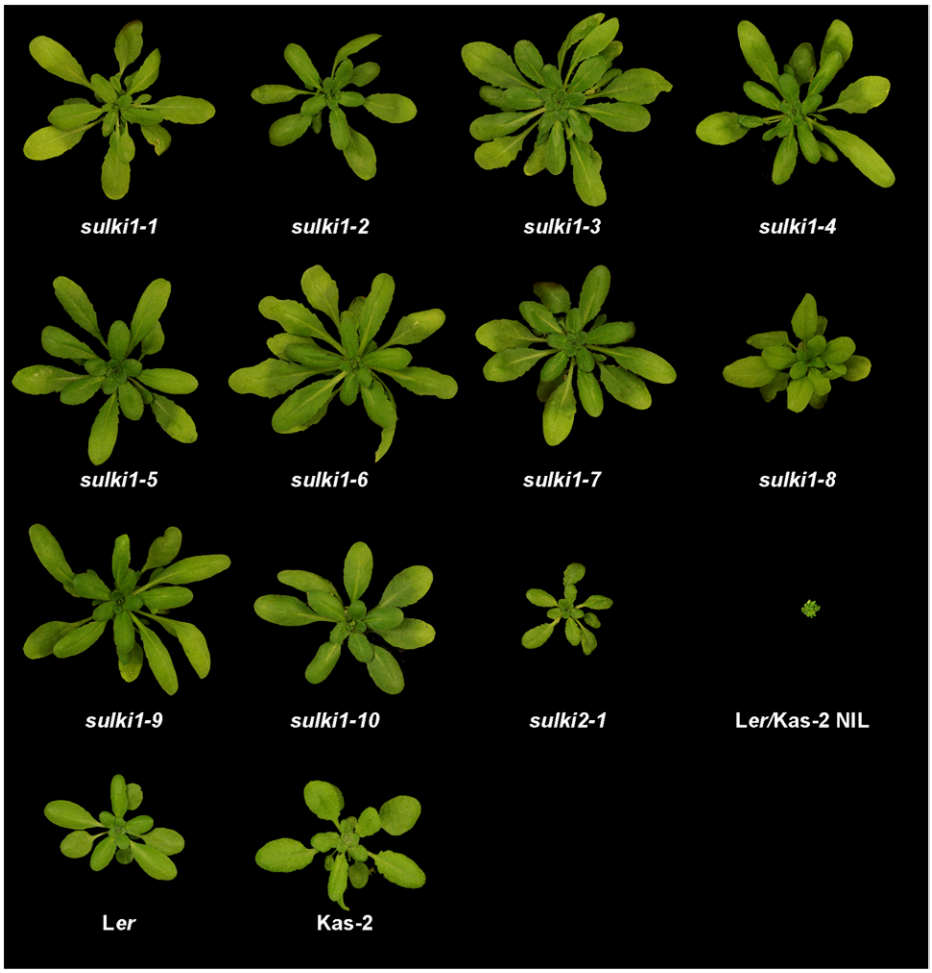

Figure 2. Composite image of *sulki* phenotypes. Five-week-old *sulki1*, *sulki2*, and L*er*/Kas2 NIL grown at 14°C to 16°C under 12-h-light/12-h-dark cycles and light intensity of 120 µmol m^{-2} s^{-1}.

incompatibility confirmed that *sulki1* mutants are allelic to Cas9-*r8*.

To confirm the causality of the *sulki2-1* mutation mapping to *RPP1-like* L*er R3*, we transformed *sulki2-1* plants with a genomic construct of *RPP1-like* L*er R3* (Alcázar et al., 2014). Complemented lines, which also were nonoverexpressors of the *RPP1-like R3* L*er* transgene, reconstituted the incompatible phenotype at 14°C to 16°C (Supplemental Fig. S6). These results are in agreement with a gene dosage effect underlying the recessive nature of the *RPP1-like* L*er* locus. In summary, we confirmed that mutations underlying *sulki1* and *sulki2*-1 suppressive phenotypes map to *RPP1-like* L*er R8* and *R3* genes, respectively.

Generation of *RPP1-Like* L*er* Loss-of-Function Mutants in L*er*/Kas2 NIL by CRISPR/Cas9

We next analyzed the contribution of other *RPP1-like* L*er* genes to L*er*/Kas2 immune-related HI by isolating CRISPR/Cas9-induced mutations in the L*er*/Kas2 NIL. Based on mRNA-seq data (see below), *RPP1-like* L*er R2*, *R3*, *R4*, and *R8* genes within the *RPP1-like* L*er* locus are predicted to encode full-length TNL proteins. *RPP1-like* L*er R1*, *R5*, *R6*, or *R7* genes contain stop codons in their TIR or NB domains. Therefore, we focused on *RPP1-like* L*er R2*, *R3*, *R4*, and *R8* to introduce frameshift mutations by CRISPR/Cas9 in TIR or NB domains. For each TNL-encoding gene, we designed protospacers next to unique NGG motifs (protospacer adjacent motif [PAM]; Fauser et al., 2014; Supplemental Fig. S4). Indel mutations resulting in early stop codons were identified in transgenic lines expressing specific *RPP1-like* L*er R2*, *R3*, *R4*, and *R8* RNA-guided endonucleases (Supplemental Fig. S4). The different mutants were then crossed with L*er*/Kas2 NIL and Cas9-free homozygous mutants isolated from the F2 progeny. To confirm the absence of mutations in other genes within the *RPP1-like* cluster, the eight *RPP1-like* L*er* genes were sequenced in the different CRISPR/Cas9 mutants (Alcázar et al., 2014).

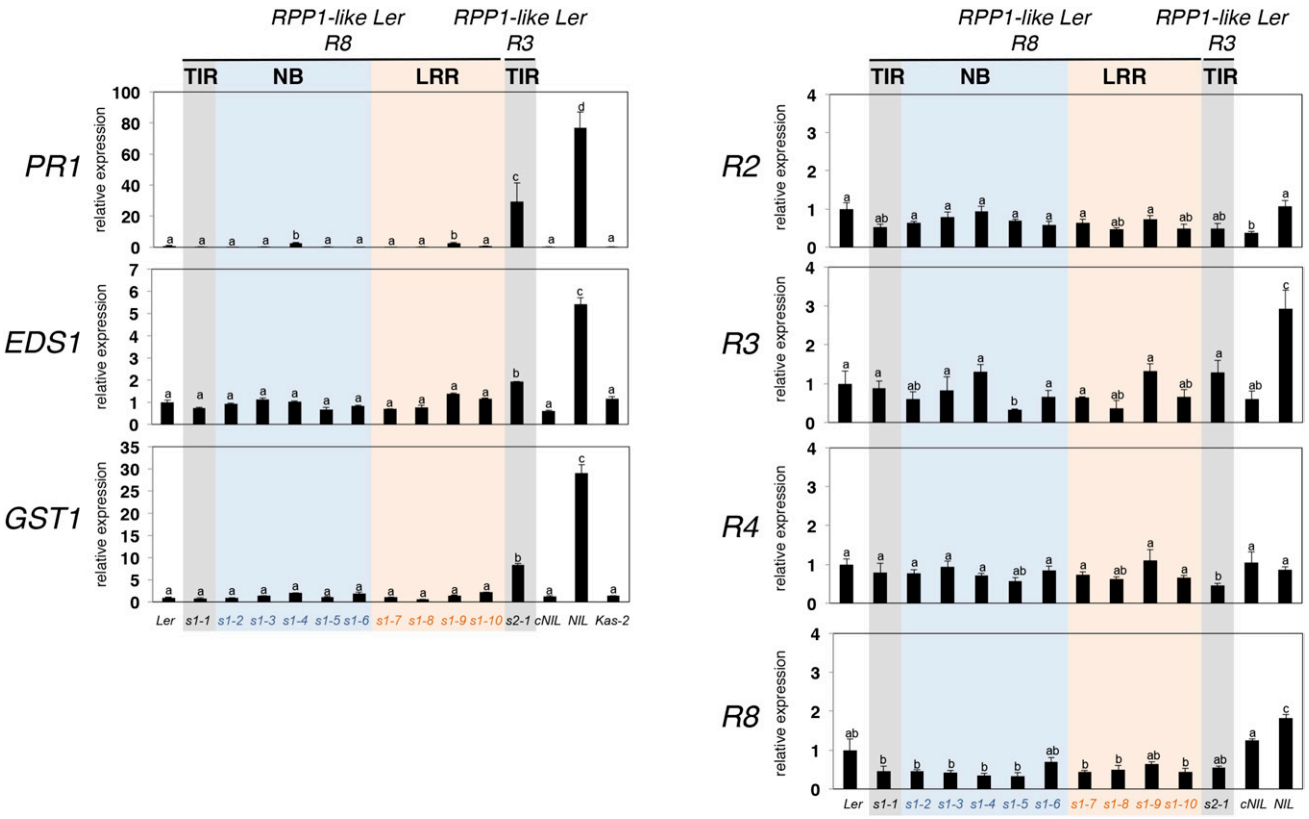

Figure 3. Expression of SA and oxidative stress marker genes. Quantitative reverse transcription PCR (RT-qPCR) analyses of *PR1*, *EDS1*, *GST1*, *RPP1-like* Ler *R2*, *R3*, *R4*, and *R8* genes in *sulki1-1* (*s1-1*) to *sulki 1-10* (*s1-10*), *sulki2-1* (*s2-1*), Ler, Kas2, Ler/Kas2 NIL, and NIL complemented with *SRF3* Ler (cNIL; Alcázar et al., 2010). Values are relative to Ler and are the mean of three biological replicates, each with three technical replicates. Letters indicate values that are significantly different according to Student-Newman-Keuls test at $P < 0.05$. Error bars indicate SD.

Loss-of-function mutations at *RPP1-like* L*er R2* (Cas9-*r2-1* and *r2-2*), *R3* (Cas9-*r3-1* and *r3-2*), and *R4* (Cas9-*r4-1* and *r4-2*) in the L*er*/Kas2 NIL were recessive and resulted in partial suppression of dwarfism and cell death (Fig. 4A; Supplemental Fig. S5; Supplemental Table S1). Lower expression of *PR1*, *EDS1*, *GST1*, and *RPP1-like* L*er R3* in 5-week-old Cas9 lines grown at 14°C to 16°C was consistent with suppression of the autoimmune response (Fig. 4B). Notably, cell death (Supplemental Fig. S5C) and *PR1*, *EDS1*, *GST1*, and *RPP1-like* L*er R3* expression (Supplemental Fig. S7) increased over time in Cas9-*r2*, *-r3* and *-r4* lines, although to a lower extent than in the L*er*/Kas2 NIL. Mutations in *RPP1-like* L*er R8* alone fully suppress incompatibility, regardless of other incompatible genes contributing to HI being present (*RPP1-like* L*er R2*, *R3*, and *R4*). Therefore, incompatibility is not simply an additive effect of various *RPP1-like* L*er* genes with *R8* having stronger effects than the others. These results indicate that *RPP1-like* L*er R2*, *R3*, and *R4* genes contribute additively to L*er*/Kas2 HI, whereas *RPP1-like* L*er R8* is epistatic to other *RPP1-like* L*er* members. Thus, additive and epistatic interactions underlie the complex nature of *RPP1-like* L*er* cluster incompatibility with Kas2. The data are consistent with the involvement of two or more *RPP1-like* L*er* genes in HI between L*er* and Kas2 (Alcázar et al., 2014; Stuttmann et al., 2016).

Bacterial Pathogen Resistance Phenotypes in *sulki1*, *sulki2*, and Cas9 *RPP1-like* L*er* Mutants

We determined the effect of *sulki1*, *sulki2*, Cas9-*r2*, Cas9-*r3*, Cas9-*r4*, and Cas9-*r8* mutations on basal disease resistance by measuring the growth of virulent *P. syringae* pv. *tomato* strain DC3000 (*Pst* DC3000) and the type III secretion-disabled *Pst hrcC* mutant, which fails to deliver virulence factors (effectors) and induces only PAMP-triggered immunity (Yuan and He, 1996). At 14°C to 16°C and 20°C to 22°C, the L*er*/Kas2 NIL exhibited higher basal resistance to *Pst* DC3000 than all other tested genotypes (Fig. 5). At both temperatures, *sulki1* and Cas9-*r8* mutations suppressed L*er*/Kas2 basal resistance to similar levels as the parents (L*er* or Kas2). By contrast, *sulki2-1*, Cas9-*r2*, Cas9-*r3*, and Cas9-*r4* mutations exhibited partial suppression of basal resistance at 14°C to 16°C but full suppression at 20°C to 22°C (similar to L*er* and Kas2). These results show that *RPP1-like* L*er R8* mutations in *sulki1*

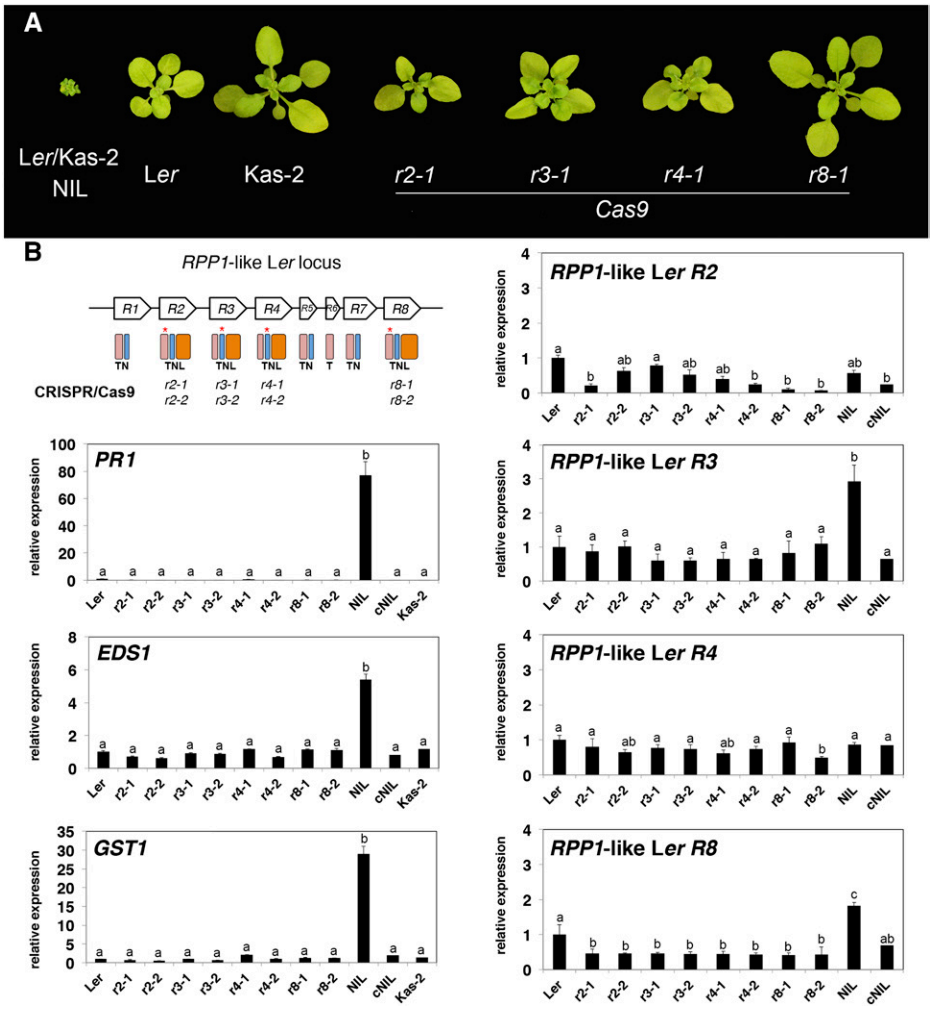

Figure 4. Growth phenotypes and expression analyses of Cas9 *RPP1*-like L*er* mutants. A, Composite image of 5-week-old Cas9-*r2-1*, Cas9-*r3-1*, Cas9-*r4-1*, Cas9-*r8-1* mutants in the L*er*/Kas2 NIL background, L*er*/Kas2 NIL, and parental lines (L*er* and Kas2) grown at 14°C to16°C. The position of stop codons in TIR (T) or NB (N) domains of *RPP1-like* genes is marked with an asterisk. B, Gene expression analyses of *PR1*, *EDS1*, *GST1*, *RPP1-like* L*er R2*, *R3*, *R4*, and *R8* in Cas9 *r2-1*, *r2-2*, *r3-1*, *r3-2*, *r4-1*, *r4-2*, *r8-1*, and *r8-2* mutant alleles L*er*, Kas2, L*er*/Kas2 NIL, and cNIL plants grown at 14°C to 16°C during 5 weeks. Analyses were performed as described in Figure 3.

and Cas9-*r8* suppress L*er*/Kas2 NIL defenses at both temperatures. A suppressive effect was observed in Cas9-*r2*, Cas9-*r3*, and Cas9-*r4* mutants only at 20°C to 22°C, consistent with their partial suppression of immune-related HI. No differences were detected between lines in response to *Pst hrcC* at either temperature (Fig. 5). Notably, mutation in *RPP1-like* L*er R8* did not lead to full susceptibility of the *eds1-2* mutant at both temperatures (Fig. 5). From these results, we concluded that suppression of *RPP1-like* L*er R8* function does not lead to a general dampening of basal defenses against *Pst* bacteria.

Gene Expression Analyses

To determine the effect of *sulki1* mutations suppressing immune-related HI on global expression profiles, we performed RNA-seq analyses in *sulki1-8*, the L*er*/Kas2 NIL, and Kas2 plants grown at 14°C to 16°C. A total of 9,564 genes exhibited significant expression differences (fold change ≥2; *P* value and false discovery rate ≤ 0.05) in the comparison between Kas2 and L*er*/Kas2 NIL (Fig. 6; Supplemental Tables 2-1 and 2-2). Of these, 5,882 genes (61.5%) were common between *sulki1-8* and L*er*/Kas2 NIL. Gene Ontology analysis of these common genes revealed an enrichment of stress-related terms (Supplemental Table S2-2). These genes represent transcriptional responses associated with incompatibility, which are suppressed in *sulki1-8*. However, 3,682 other genes were still differentially expressed in the comparison between Kas2 and L*er*/Kas2 NIL. These expression changes might be due to differences in the genetic background between Kas2 and the L*er*/Kas2 NIL not associated with incompatibility

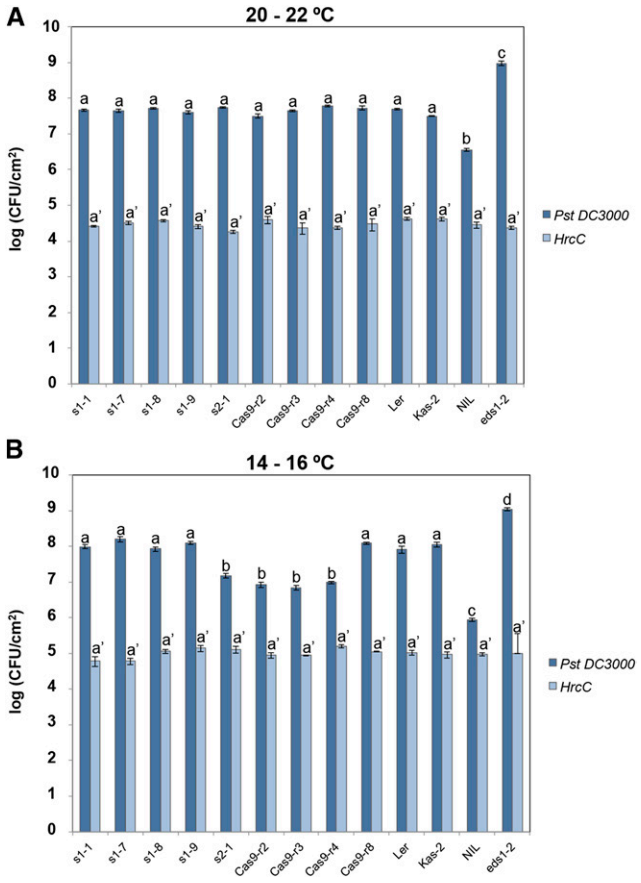

Figure 5. Growth of *Pst* DC3000 and *hrcC* mutant, 3 d after spray inoculation of *sulki1-1* (*s1-1*), *sulki1-7* (*s1-7*), *sulki1-8* (*s1-8*), *sulki1-9* (*s1-9*), *sulki2-1* (*s2-1*), Cas9- *r2-1*, *r3-1*, *r4-1*, and *r8-1* mutants in the L*er*/Kas2 NIL background, L*er*, Kas2, L*er*/Kas2 NIL, and *eds1-2* L*er* plants grown at 20°C to 22°C (A) or 14°C to 16°C (B). Different letters indicate significant differences ($P < 0.01$) in a Student-Newman-Keuls test. Error bars indicate SD.

(Supplemental Table S2-1). Gene Ontology analysis in this subset of genes identified an enrichment of nitrogen metabolism-related terms (Supplemental Table S2-1). Finally, RNA-seq analysis identified 622 other genes differentially expressed in *sulki1-8* versus L*er*/Kas2 NIL that did not show significant expression differences in Kas2 versus L*er*/Kas2 NIL. These *sulki1-8*-specific genes were related to oxidation-reduction based on Gene Ontology (Supplemental Table S2-3).

Global Metabolite Profiling

We determined the effects of *sulki1* mutations on primary metabolism through global metabolite profiling by gas chromatography/mass spectrometry (GC/MS) in L*er*/Kas2 NIL, *sulki1* (*sulki1-1*, *sulki1-7*, *sulki1-8*, and *sulki1-9*) and the parents (L*er* and Kas2) at 14°C to 16°C. The metabolomics analysis identified 57 metabolites in the analyzed samples, 36 of which were consistently detected in all genotypes and used for principal component analysis (PCA; Fig. 7A). The nature of 23 of these 36 metabolites was known and annotated according to the MPIMP-Golm inventory list (Kopka et al., 2005). Among the identified metabolites, we detected amino acids, polyhydroxy acids, sugars, and TCA cycle intermediates (Supplemental Table S3). In the PCA analysis, PC1 explained 50.3% of the total variance and differentiated between the incompatible L*er*/Kas2 NIL and other genotypes. PC1 indicated that the *sulki1* mutations cause a reversal of a large part of the altered primary metabolome in L*er*/Kas2 NIL to L*er* or Kas2 parent levels. This metabolic reversal was consistent with suppression of the dwarf phenotype (Fig. 2), the absence of cell death at low temperature (Supplemental Fig. S1B), and deactivation of transcriptional defense responses (Fig. 3) in the *sulki* mutants. Conversely, PC2 (21.9% of the total variance) revealed that some metabolic differences remained between *sulki1* mutants or L*er*/Kas2 NIL and the parents (Fig. 7A; Supplemental Table S4).

Hierarchical cluster analysis (HCA) with Pearson's correlation and average linkage of metabolites and genotypes identified metabolic differences between the strongly deviating L*er*/Kas2 NIL, the parents, and the *sulki1* mutants (Fig. 7B). The heat map representation indicated a large cluster of metabolites that differentially accumulated in L*er*/Kas2 NIL (Fig. 7B). Compared with L*er* and Kas2, the incompatible L*er*/Kas2 NIL accumulated amino acids, such as Gln/pyro-Glu, Asp, Thr, or Ala, lipid-related phosphate, glycerol, ethanolamine, carbohydrate metabolism related glyceric acid, Glc-6P, and Suc (Fig. 7C). The levels of ascorbate, a substrate of the glutathione-ascorbate cycle for hydrogen peroxide detoxification, were much lower in L*er*/Kas2 NIL than in the isogenic Kas2, consistent with the occurrence of oxidative stress induced by HI. On the other hand, dehydroascorbate levels were similar in the two genotypes. These metabolic changes appear to be associated with HI, specifically with growth reduction in combination with metabolic recycling caused by the increased frequency of cell death in L*er*/Kas2 NIL leaf tissue.

As expected, most metabolic reprogramming associated with HI was reverted in *sulki1* mutants to Kas2 levels, e.g. ascorbate, Suc, phosphate, glycerol, Asp, Gln/pyro-Glu, and Thr (Fig. 7C). However, *sulki1* mutants exhibited metabolic changes that differed from L*er*/Kas2 NIL, L*er*, or Kas2 (Fig. 7C). These changes in the *sulki1* mutants might be linked to *RPP1-like* L*er* *R8*-independent transcriptional defense activation (Fig. 6). Levels of Glu, Asp, Thr, Ala, and dehydroascorbate were lower than in the parents. In parallel, Glc and Fru levels were consistently higher in *sulki1-1*, *sulki1-7*, *sulki1-8*, and *sulki1-9* compared to the parents L*er*, Kas2, and the incompatible L*er*/Kas2 NIL. However, such differences were not observed in the levels of Suc or Glc-6P (Fig. 7C). Quantification of starch at the end of the day (light) and before dawn (dark) in the above genotypes indicated the lower capacity of L*er*/Kas2 NIL to accumulate starch during the day, although its

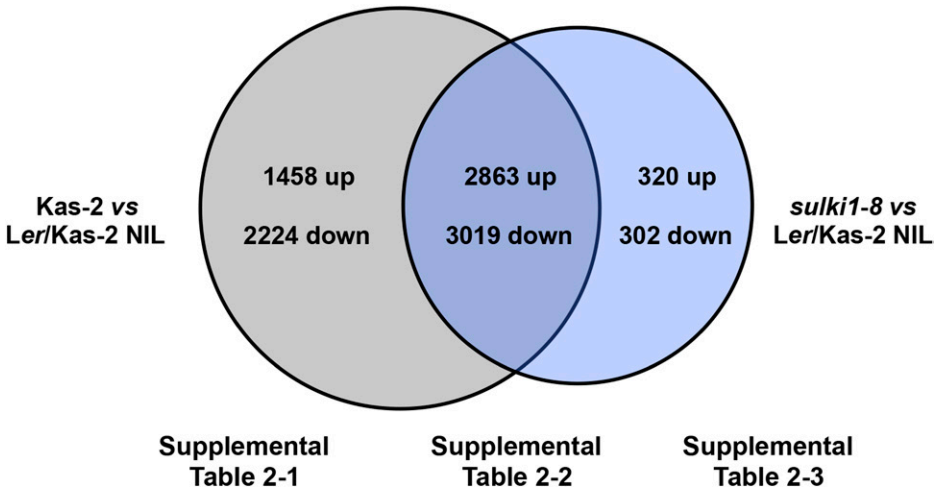

Figure 6. Venn diagram of genes differentially expressed in the comparisons between (Kas2 versus L*er*/Kas2 NIL) and (*sulki1-8* versus L*er*/Kas2 NIL). Lists of genes and Gene Ontology analyses are included in Supplemental Tables S2-1 to S2-3.

levels were not depleted at dawn (Supplemental Fig. S8). Interestingly, the L*er*/Kas2 NIL also exhibited higher apoplastic invertase activity than L*er*, Kas2, or *sulki1*, whereas vacuolar invertase was barely affected (Supplemental Fig. S9). These results can be explained by the suggested role of cell wall invertase in plant defense (Tauzin and Giardina, 2014). The absence of Glc or Fru accumulation in the L*er*/Kas2 NIL, despite the presence of high apoplastic invertase activity, suggests the use of carbohydrates in the biosynthesis of secondary metabolites involved in defense or cell wall strengthening. These demands might contribute to the metabolic costs of diverting resources away from growth in the L*er*/Kas2 NIL.

All together, global metabolite profiling confirmed a physiological reversal of the L*er*/Kas2 HI metabolic phenotype in *sulki1*. It also reinforced *RPP1-like* L*er* *R8*-independent responses at a metabolic level that were indicated by transcriptome profiling (Fig. 6). We concluded that the L*er*/Kas2-incompatible hybrids are growth inhibited, but that this inhibition is likely not due to limited C, N, or P resources.

Characterization of a Pathogenic *Hpa* Isolate in the Arabidopsis Gorzów Population

Previously, we collected a population of L*er* relatives (Gw) in Gorzów Wielkopolski (Poland), in which 30% of individuals carried a conserved *RPP1-like* L*er* haplotype (Alcázar et al., 2014). In 2014, we revisited the population site and isolated *Hpa* naturally infecting Gw plants, for which a basic population structure was already established (Alcázar et al., 2014). *Hpa* was found sporulating on cauline leaves of the susceptible genotype Gw-16. We refer to this local oomycete as *Hpa* Gw, which was propagated as a mass conidiospore culture from a single plant. The *Hpa ATR1* gene, encoding an effector recognized by certain *RPP1-like* TNL receptors, was used to establish a phylogenetic relationship between *Hpa* Gw and other known *Hpa* isolates. Sequencing of *ATR1* from *Hpa* Gw did not identify segregating polymorphisms within this population, which would be indicative of mixed *Hpa* populations. *Hpa* Gw was found to be more related to *Hpa* isolate Cala2 and Emwa1 than other *Hpa* isolates (Supplemental Fig. S10).

Examination of *Hpa* Gw disease resistance in 40 genetically different Arabidopsis Gw lines identified seven genotypes (17.5%) that were susceptible to *Hpa* Gw (e.g. Gw-16 in Supplemental Fig. S11; Supplemental Table S5). The remaining genotypes, as well as L*er*, Col-0, Kas2, L*er*/Kas2 NIL, and cNIL (Alcázar et al., 2010) exhibited a HR indicative of resistance to *Hpa* Gw infection and consistent with host *RPP*-mediated pathogen recognition (Supplemental Fig. S11). T-DNA insertion mutants of *RPP1* and *RPP1-like* genes in Col-0 *At3g44400* (N632237 and N518157), *At3g44480* (N599581 and N655327), *At3g44630* (N644159 and N658450), and *At3g44670* (N529707 and N477722) did not support the growth of *Hpa* Gw and exhibited HR (Supplemental Fig. S11). Susceptible and resistant Gw genotypes were not differentiated from each other in PCA analyses based on 134 genome-wide distributed SNPs (Alcázar et al., 2014; Supplemental Fig. S12). Notably, however, all genotypes carrying the conserved *RPP1-like* L*er* haplotype were resistant to *Hpa* Gw infection (Supplemental Fig. S12; Supplemental Table S5). Despite this, resistance is not strictly associated with the presence of an *RPP1-like* L*er* haplotype because it is expressed in accessions that do not carry the haplotype (e.g. Col-0).

Effect of Suppressive Mutations on *Hpa* Gw Disease Resistance in L*er*/Kas2 NIL

Next, we studied the effect of the L*er*/Kas2 HI suppressor (*sulki*) mutations on resistance to the local *Hpa* Gw isolate in the L*er*/Kas2 NIL. For this, we inoculated Cas9-*r2*, Cas9-*r3*, Cas9-*r4*, Cas9-*r8*, *sulki1* (*sulki1-3*, *sulki1-7*, *sulki1-8*, *and sulki1-9*), *sulki2-1*, and *near death experience1-3* (*nde1-3*), which carries a deletion between *RPP1-like R3-R8* L*er* genes (Stuttmann et al., 2016).

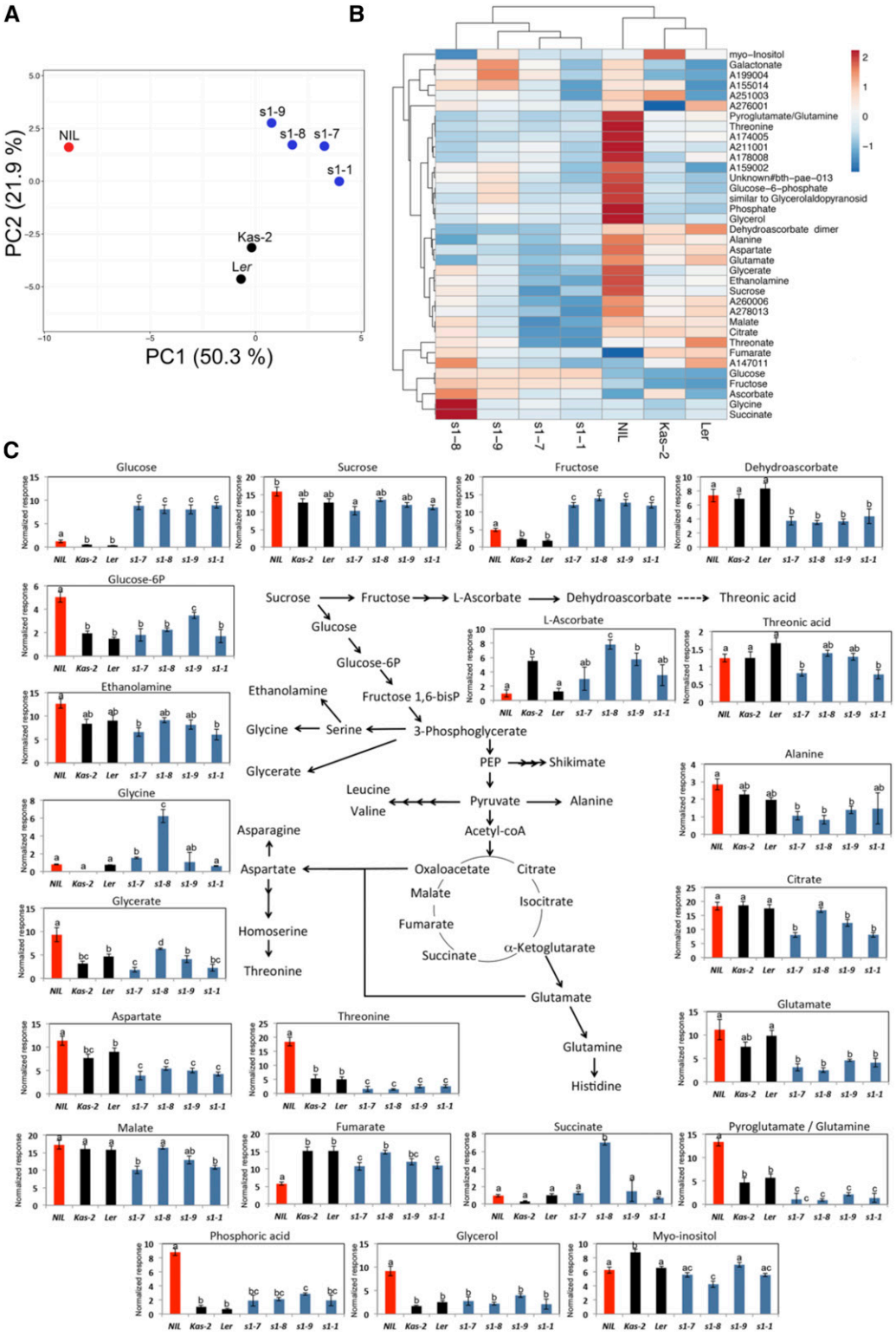

Figure 7. Principal component analysis (A) and HCA (B) with Pearson's correlation and average linkage of samples and metabolites from 5-week-old *sulki1-1* (*s1-1*), *sulki1-7* (*s1-7*), *sulki1-8* (*s1-8*), *sulki1-9* (*s1-9*), L*er*, Kas2, and L*er*/Kas2 NIL plants grown at 14°C to16°C. C, Log_2-normalized responses for some metabolites determined by GC/MS in the above genotypes, and schematic representation of their metabolic pathways. Different letters indicate significant differences ($P < 0.01$) in a Student-Newman-Keuls test. Error bars indicate SD. A complete list of analyzed metabolites is provided in Supplemental Table S3.

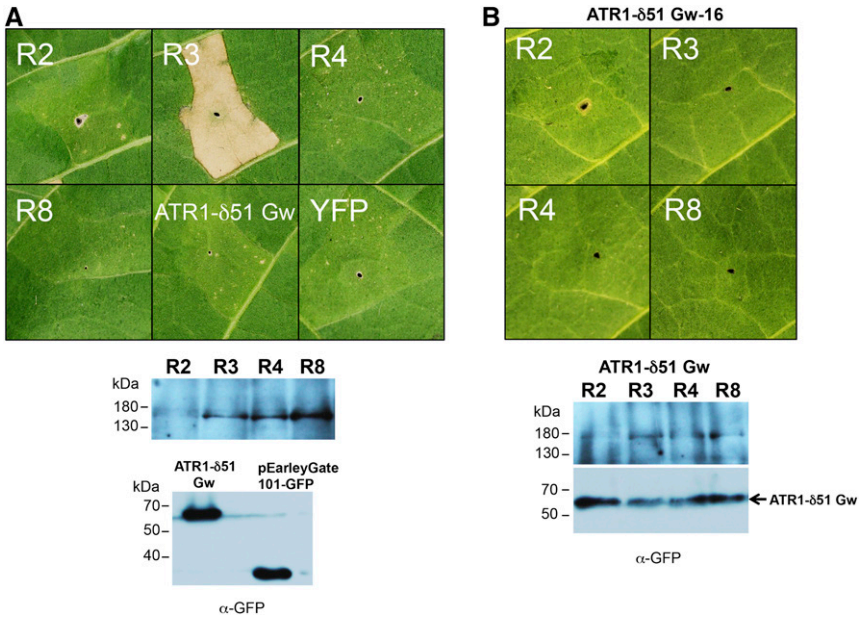

Figure 8. Transient expression assays in tobacco. A, Transient expression of genomic versions of 35s: *RPP1-like* L*er R2*, *R3*, *R4*, *R8*, and ATR1-*δ*51 Gw, tagged with C terminus YFP. B, Coinfiltration of *RPP1-like* L*er R2*, *R3*, *R4*, and *R8* with ATR1-*δ*51 Gw. Pictures in A and B were taken 48 h after infiltration. Samples for western-blot analyses in A and B were collected 24 h after infiltration. No symptoms of cell death were observed at later time points of coinfiltration in B.

Resistance to *Hpa* Gw was observed in all genotypes tested (Supplemental Fig. S11). We concluded that mutations suppressing L*er*/Kas2 incompatibility do not compromise disease resistance to a local *Hpa* isolate.

Analysis of ATR1 Gw Recognition by RPP1-Like L*er* Proteins in Tobacco

RPP1-like TNL receptors directly recognizing ATR1 effector variants from different *Hpa* isolates have been characterized (Rehmany et al., 2005; Sohn et al., 2007; Krasileva et al., 2010). We determined the capacity of TNL RPP1-like L*er* R2, R3, R4, and R8 proteins to recognize ATR1 cloned from Gw leading to cell death in tobacco transient expression assays. For this, C-terminal YFP fusions of *RPP1-like* L*er R2*, *R3*, *R4*, *R8* genomic constructs, and ATR1-*δ*51 *Hpa* Gw (lacking the ATR1 secretory signal peptide; Steinbrenner et al., 2015) were generated for *Agrobacterium tumefaciens* infiltration of tobacco leaves. Accumulation of *RPP1-like* L*er* R3 protein over a threshold triggered cell death in tobacco leaves (Fig. 8A), consistent with L*er*/Kas2 NIL phenotypes induced by *R3* overexpression in Arabidopsis (Alcázar et al., 2014) and its involvement in L*er*/Kas2 immune-related HI (Fig. 4). However, 1:1 coinfiltration of *δ*51-ATR1 *Hpa* Gw with *RPP1-like* L*er* R2, R3, R4, or R8, which resulted in lower but detectable RPP1 protein expression in tobacco leaves, did not induce cell death (Fig. 8B). These results suggest that ATR1 *Hpa* Gw is not recognized by any of the RPP1-like L*er* variants tested.

Hpa Gw Disease Resistance Is Independent of *EDS1*- and *ICS1*-Generated SA

We tested whether resistance to *Hpa* Gw was compromised in *eds1-2* (Col-0; Bartsch et al., 2006), *eds1-2*; L*er*; Feys et al., 2005), the SA-deficient *ISOCHORISMATE SYNTHASE1 sid2-1* mutant (Col-0; Wildermuth et al., 2001), or L*er-NahG* transgenic plants that metabolize SA into catechol (Bowling et al., 1994). Neither *eds1-2* nor SA depletion affected resistance to *Hpa* Gw (Supplemental Fig. S11). Because *TNL immunity* relies on *EDS1* (Aarts et al., 1998; Feys et al., 2001, 2005) and the *RPP1-like* L*er* locus only contains *TNL* genes (Alcázar et al., 2009), we reasoned that resistance to *Hpa* Gw is governed by other *RPP* loci in the genome.

Mapping of *Hpa* Gw Disease Resistance

Whereas L*er* is resistant to *Hpa* Gw, we found that the Shakdara (Sha) accession is susceptible, which enabled us to exploit a L*er*/Sha recombinant inbred line (RIL) population (Clerkx et al., 2004) in QTL mapping of *Hpa* Gw resistance loci (Supplemental Table S6). QTL analyses identified one major-effect QTL on chromosome 1 explaining 52% of the phenotypic variation, with L*er* alleles contributing most resistance to isolate *Hpa* Gw. L*er*/Sha RILs carrying Sha alleles at this QTL but L*er* alleles at the *RPP1-like* locus were susceptible to *Hpa* Gw infection (Supplemental Table S6). Therefore, the *RPP1-like* L*er* locus does not confer resistance to *Hpa* Gw. The QTL spanned 2.83 Mb between markers F6D8-94 and GENEA. This region contains at least nine *CNL*

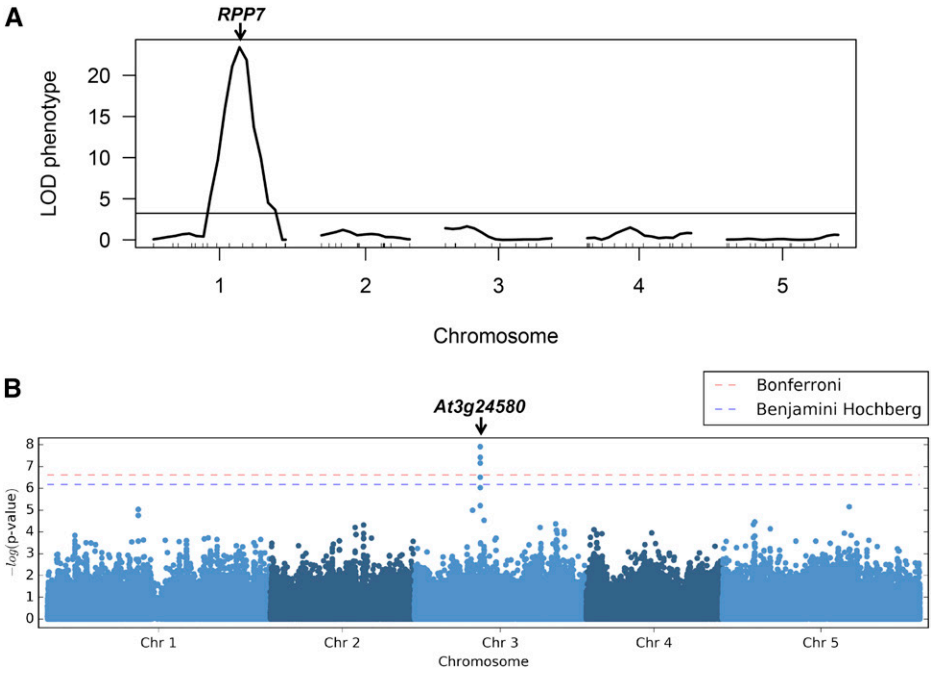

Figure 9. QTL and GWAS mapping. A, QTL mapping of disease resistance to *Hpa* isolate Gw in the L*er*/Sha RIL population (Clerkx et al., 2004; see Supplemental Table S6). The position of *RPP7* on chromosome 1 is indicated. B, Manhattan plot of GWAS mapping for disease resistance to *Hpa* Gw in 288 accessions (see Supplemental Table S8). The list of most significant gene associations is shown in Supplemental Table S9.

genes, among them *RPP7* (*At1g58602*; Supplemental Table S7), which was reported to confer resistance to *Hpa* isolate Hiks1 in an SA- and *EDS1*-independent manner (McDowell et al., 2000; Fig. 9A). Therefore, we consider *RPP7* as a strong candidate gene in L*er* resistance to *Hpa* Gw.

In addition to QTL analyses, we performed GWAS mapping using 288 Arabidopsis accessions distributed worldwide. Of the total phenotyped accessions, 78 (27%) were susceptible to *Hpa* Gw infection. Disease resistance phenotypes did not follow obvious geographical or population structure patterns and were segregated between and within populations (Supplemental Table S8). GWAS analysis for *Hpa* Gw disease resistance identified a significant association with multiple SNPs belonging to gene *At3g24580*, encoding an F-box protein of unknown function (Fig. 9B; Supplemental Table S9). However, no genetic variation at *At3g24580* was found between *Hpa* Gw-resistant (Gw-30, Gw-31, Gw-112, Gw-127, and Gw-144) and -susceptible (Gw-16, Gw-50, Gw-107, Gw-148, and Gw-167) genotypes, which all carried *At3g24580* Col-0 alleles (Supplemental Table S5). We concluded that *At3g24580* does not condition differences in disease resistance to *Hpa* Gw in the Gorzów population, although its epistatic interaction with other genes cannot be excluded in other genetic backgrounds. Together, the QTL and GWAS mapping identified candidate *RPP* genes outside the *RPP1-like* locus as conferring resistance to *Hpa* Gw.

DISCUSSION

Epistasis, defined as the nonadditive interaction between mutations, is the basis for many postzygotic immune-related HI in plants (Bomblies, 2010). The environment can affect the consequences of epistasis on fitness (Flynn et al., 2013). Indeed, growth defects in L*er*/Kas2 NIL at 14°C to 16°C are suppressed at 20°C to 22°C (Alcázar et al., 2009), a temperature at which basal disease resistance to *Pst* DC3000 is retained (Fig. 5). HI is not the result of direct action by natural selection but rather a byproduct of divergence through evolutionary processes acting on other traits (Coyne and Orr, 2004). Selective forces acting on *R* genes involve arms races between plants and pathogens, in addition to environmental factors (Dodds and Rathjen, 2010; Ariga et al., 2017). Such divergence might thus be shaped by adaptation to different environments (ecological speciation) or through different pathways within the same environment (Sherlock and Petrov, 2017). Adaptive mutations increasing fitness can be retrieved by experimental evolution, an approach facilitated by the study of microbial populations during multiple generations. In yeast, adaptation to divergent and identical environments has been shown to promote the emergence of reproductive isolation (Dettman et al., 2007; Ono et al., 2017). However, the intrinsic lethal nature of incompatible hybrids hinders the identification of potential mutations suppressing negative epistasis. Here, we circumvented this limitation by inducing random and

CRISPR/Cas9-guided mutagenesis in a large population of L*er*/Kas2 NIL plants. Through this approach, we identified *RPP1* intragenic mutations that suppress L*er*/Kas2 immune-related HI and observed different degrees of phenotypic adaptation.

The mutagenesis screen identified a large number of intragenic *suppressors of Ler/Kas2 incompatibility* (*sulki*) mapping to *RPP1-like* L*er R8* (*sulki1-1* to *sulki1-10*) and one mutation mapping to *RPP1-like* L*er R3 (sulki2-1)* that suppressed HI (Fig. 2). Due to the presence of moderate suppressor phenotypes in the EMS population, we reasoned that intragenic mutations leading to intermediate phenotypes might have been overlooked, including mutations in other potential *RPP1-like R3* alleles. Therefore, to provide a comprehensive analysis of the *RPP1-like* L*er* locus, we mutated each *RPP1-like* L*er* TNL encoding gene by CRISPR/Cas9 in the L*er*/Kas2 NIL background (Cas9-*r2*, Cas9-*r3*, Cas9-*r4*, and Cas9-*r8*) and studied the effects of the mutations on growth, cell death, gene expression, and disease resistance. EMS and CRISPR/Cas9 mutagenesis revealed epistatic interactions between *RPP1-like* L*er R8* and other *RPP1-like* L*er* members (*R2*, *R3*, and *R4*), with the latter contributing additively to immune-related HI (Fig. 4). These results are consistent with the involvement of two or more *RPP1-like* genes in L*er*/Kas2 incompatibility and suggest coaction between *RPP1-like* members for defense activation in Arabidopsis (Alcázar et al., 2014). The dominant nature of *RPP1-like* L*er R8* loss-of-function mutations suggests that a certain dosage of incompatible RPP1-like protein is required for the autoimmunity phenotype, and loss-of-function alleles in *RPP1-like* L*er R8* lower this dosage below a critical level when heterozygous. This might also explain the recessive nature of the *RPP1-like* haplotype in L*er*/Kas2 immune-related HI (Alcázar et al., 2009, 2014).

L*er*/Kas2 HI suppressor mutations mapped to different domains of *RPP1-like* L*er R8* (Fig. 1). The different mutations behaved like Cas9-*r8* loss-of-function alleles, indicating that *sulki1* mutations disrupt *RPP1-like* L*er R8* function in L*er*/Kas2 HI (Fig. 4). RNA-seq analyses in *sulki1-8* show that many transcriptional changes in incompatible L*er*/Kas2 hybrids are suppressed by *RPP1-like* L*er R8* mutation. However, the expression of other genes related with oxidation reduction was modified in *sulki1-8* mutants compared to its isogenic Kas2 genotype (Fig. 6; Supplemental Tables S2-1 to S2-3). The occurrence of these *RPP1-like* L*er R8*-independent expression sectors supports a multigenic basis for the *RPP1-like* L*er*-incompatible haplotype. Importantly, such expression sectors alone are not sufficient to trigger incompatibility, which requires a functional R8 protein.

Most *sulki1* suppressor mutations in *RPP1-like* L*er R8* were found in NB- or LRR-domain-conserved motifs and invariable residues. The NB-ARC domain is involved in nucleotide binding and hydrolysis and acts as a molecular switch for NLR activation (van Ooijen et al., 2008; Takken and Goverse, 2012). The NB-ARC is required for RPP1 self-association and cell death activation, probably assisted by TIR-TIR interactions (Schreiber et al., 2016). The LRR domain of TNL proteins is often involved in effector recognition, inducing a conformational change that switches the protein to an active state (van Ooijen et al., 2008; Takken and Goverse, 2012; Steinbrenner et al., 2015). Nonsynonymous substitutions in the LRR domain of *DM2h* Bla-1 are responsible for incompatibility with *DM1* Hh-0. Certain ATR1 alleles from *Hpa* isolates are recognized by the LRR domain of *RPP1* Ws-0 and Nd-1 (Krasileva et al., 2010; Steinbrenner et al., 2015). The identification of *DM2h* Bla-1 incompatible-trigger mutations in the *LQQL* motif of LRR4, next to a modeled ATR1 docking site, suggested that incompatible *RPP1* variants originate from an arms race between the immune receptor and pathogen ligands (Chae et al., 2014). Notably, the *sulki1-9* mutation (R821H) in LRR5 of *RPP1-like* R8 L*er* is adjacent to this *LQQL* motif (Fig. 1). A frameshift mutation in LRR2 of *RPP1-like* L*er R8* in the *nde1-1* mutant also suppresses incompatibility with Kas2. The *nde1-1* mutant was isolated from a suppressor screen for autoimmune phenotypes associated with EDS1 nuclear enrichment and suggested a role for *RPP1-like* L*er R8* in EDS1/PAD4 defense amplification (Stuttmann et al., 2016). Thus, polymorphism at the LRR domain of *RPP1-like* L*er R8* and its homolog in Bla-1 (*DM2h*) seems to be relevant for incompatibility (Chae et al., 2014; Stuttmann et al., 2016).

Here, we find that mutations in the TIR domains of RPP1-like L*er R3* and *R8* also suppress L*er*/Kas2 immune-related HI (Fig. 1). The TIR domain is necessary for receptor signaling, and in some TNLs, including RPP1, this domain self-associates and is sufficient for triggering cell death (Swiderski et al., 2009; Bernoux et al., 2011; Williams et al., 2014; Steinbrenner et al., 2015; Schreiber et al., 2016; Zhang et al., 2017). Whether *sulki1-1* and *sulki2-1* mutations disrupt potential self-association of *RPP1-like* L*er* R3 or R8 proteins needs to be determined.

We investigated whether the *RPP1* L*er* genes contributing to HI also participate in *Hpa* Gw recognition (Krasileva et al., 2010; Steinbrenner et al., 2015). Our analysis, using a local *Hpa* Gw isolate, indicated that the incompatible *RPP1* L*er* haplotype does not contribute to disease resistance to this local pathogen and that the resistance is SA and *EDS1* independent (Supplemental Fig. S11). Furthermore, we found that coexpression of *RPP1-like* L*er* R2, R3, R4, or R8 proteins with ATR1-δ51 *Hpa* Gw did not trigger HR in tobacco transient expression assays (Fig. 8B). Moreover, QTL mapping in the L*er*/Sha RIL population identified a major QTL on chromosome 1 that contained L*er* alleles contributing to resistance (Fig. 9A). The QTL interval spanned several *R* genes, including *RPP7*, a known *CNL* gene governing resistance to the *Hpa* Hiks1 isolate in an SA- and *EDS1*-independent manner (McDowell et al., 2000; Supplemental Table S7). From these data, we concluded that the incompatible *RPP1-like* L*er* haplotype does not contribute to disease resistance to a local *Hpa* isolate. Also, intragenic

mutations suppressing L*er*/Kas2 incompatibility do not incur on a fitness cost in terms of *Hpa* resistance (Supplemental Fig. S11). However, such mutations dampen disease resistance to *Pst* DC3000 of the L*er*/Kas2 NIL at 20°C to 22°C (Fig. 5), which might represent a trade-off between growth and basal defenses against virulent leaf-colonizing *P. syringae* bacteria.

Hpa populations might have diverged or even been extinguished since the birth of the *RPP1-like* L*er* haplotype, which was already present in the Gorzów population in 1939 (Alcázar et al., 2014). Thus, the contemporary *Hpa* Gw isolate might not represent a selective force for the *RPP1-like* L*er*-incompatible haplotype. However, fine-tuning *RPP1-like* L*er R3* expression may benefit disease resistance to other pathogenic strains (Alcázar et al., 2014), thereby favoring selection of the incompatible haplotype. Interestingly, *RPP1-like* L*er R3* and *R4* are homologs of *At3g44400* Col-0 (Alcázar et al., 2014) and whole-genome sequencing revealed the absence of *At3g44400* Col-0 gene in L*er* (Supplemental Fig. S13). This suggests that *RPP1-like R3* and *R4* in L*er* are derived from a gene transposition and duplication event from *At3g44400* during the formation of the incompatible *RPP1-like* haplotype.

Incompatible L*er*/Kas2 NIL plants exhibit metabolic hallmarks of HI, which can be explained by a combination of growth arrest and metabolic recycling of material from dead or dying leaf cells. Recycling likely also involves proteolysis and triglyceride degradation accompanied by oxidative stress (Fig. 7C). We further detected a promotion of Suc degradation through cell wall invertase, but not vacuolar invertase activities (Supplemental Fig. S9). Activation of cell wall invertase is triggered by defense responses to various pathogens, including oomycetes and bacteria (Tauzin and Giardina, 2014). Glc and Fru can be used as carbon sources for the biosynthesis of defense-related metabolites, potentially leading to a metabolic cost that reduces growth in the dwarf L*er*/Kas2 NIL (Bolton, 2009). Remarkably, these metabolic costs are fully suppressed in *sulki1* mutants, which also suppress oxidative stress symptoms. Nevertheless, *sulki1* mutants accumulate higher levels of Glc, Fru, and starch than the L*er*/Kas2 NIL (Fig. 7C), possibly due to *RPP1-like* L*er R8*-independent transcriptional activation of defense responses.

Our data shed light on the complex genetic nature of the *RPP1-like* L*er* locus triggering incompatibility with Kas2. Through random and guided mutagenesis, mutations can be generated that mitigate fitness costs of L*er*/Kas2 HI, while retaining resistance to a local *Hpa* Gw isolate. However, trade-offs are also inherent to such compensatory mutations.

MATERIALS AND METHODS

Plant Material and Growth Conditions

A complete list of Arabidopsis (*Arabidopsis thaliana*) accessions used in this study is provided in Supplemental Table S8. Seeds were obtained from the Nottingham Arabidopsis Stock Center or collected by authors (Alcázar et al., 2014). The incompatible L*er*/Kas2 NIL and cNIL used in this study were described previously (Alcázar et al., 2009, 2010). Plants were grown on soil at indicated temperatures under 12-h-dark/12-h-light cycles and 70% relative humidity and 120 µmol m^{-2} s^{-1} of light intensity.

EMS Mutagenesis

Seeds of L*er*/Kas2 NIL were soaked overnight in 1 mg/mL KCl at 4°C. After seed imbibition, the solution was discarded and replaced with 0.2% EMS (v/v) and incubated for 16 h. Seeds were then washed 10 times with 50 mL of water and suspended in 0.1% agarose for sowing on soil. Approximately 25,000 M1 plants were allowed to self at 20°C to 22°C. M2 seeds were collected in pools of 100 to 150 M1 plants. M2 plants were grown at 14°C to 16°C to identify suppressors of L*er*/Kas2 incompatibility (*sulki*).

Whole-Genome Sequencing

Genomic DNA from Arabidopsis plants was extracted from leaves of 5-week-old plants grown on soil using the CTAB method (Doyle, 1991). DNA quality was checked on 0.8% agarose gel electrophoresis stained with ethidium bromide. DNA concentration was determined by fluorometric quantitation using the dsDNA HS assay kit and the Qubit device (Thermo Fisher). Whole-genome sequencing was performed at the Centro Nacional de Análisis Genómico (CNAG, Spain). A standard Illumina protocol was followed to create paired-end libraries, which were run on Illumina sequencers HiSeq 3000/4000 2x150 according to standard procedures. Sample statistics are shown in Supplemental Table S10. Read mapping and variant detection were performed using the CLC Genomics Workbench 10 version 10.1.1 (Qiagen).

RT-qPCR Expression Analyses

Total RNA was extracted using Trizol reagent (Thermo Fisher). Reverse transcription and quantitative real-time PCR was performed as described (Alcázar et al., 2014). A complete list of primers used for expression analyses is reported in Alcázar et al. (2014).

RNA-Seq Expression Analyses

Total RNA was extracted from fully expanded leaves of 5-week-old *sulki1-8*, Kas2, and L*er*/Kas2 NIL plants grown at 14°C to 16°C. Three biological replicates, each from pooled leaves of at least three independent plants grown in individual pots were used for the analysis. Total RNA was extracted using Trizol (Thermo Fisher), quantified in a Nanodrop ND-1000 spectrophotometer, and checked for purity and integrity in a Bioanalyzer-2100 device (Agilent Technologies). RNA samples were further processed by the CNAG (Spain) for library preparation and RNA sequencing. Libraries were prepared using the Illumina TruSeq Sample Preparation Kit according to the manufacturer's instructions. Each library was paired-end sequenced (2 × 75 bp) on HiSeq 2000 Illumina sequencers. Sample statistics are shown in Supplemental Table S10. Read mapping and expression analyses were performed using the CLC Genomics Workbench 10 version 10.1.1 (Qiagen). Only significant expression differences (fold change ≥ 2; *P* value and false discovery rate ≤ 0.05) were considered.

CRISPR/Cas9 Mutagenesis

To identify specific PAM motifs in *RPP1-like* L*er* genes, their sequences were aligned using multiple sequence comparison by Log-Expectation (http://www.ebi.ac.uk/Tools/msa/muscle/) and unique NGG motifs identified in TIR or NB domains of *RPP1-like* L*er R2*, *R3*, *R4*, and *R8*. Generation of CRISPR/Cas9 lines was based on the system reported by Fauser et al. (2014). Spacers were designed next to unique PAM sites and annealed oligonucleotides containing *Bbs*I sites were used for the generation of customized RNA chimeras in the pEn-Chimera vector (Supplemental Table S11). The customized RNA chimeras were transferred into pDe-CAS9 by Gateway LR reaction (Thermo Fisher). The final clones were sequenced and transformed into *Agrobacterium tumefaciens* GV3101 pMP90. L*er*/Kas2 NIL plants were transformed by floral dipping and transgenic lines isolated by selection with 20 µg/mL

glufosinate-ammonium (Sigma-Aldrich). Individual lines were checked for the presence of indel mutations by SANGER sequencing of all *RPP1-like* L*er* genes (Alcázar et al., 2014), crossed to L*er*/Kas2 NIL, and Cas9-free homozygous mutants isolated in the F2 by gene sequencing and Cas9 genotyping (Supplemental Table S11).

Histochemical Analyses and Determination of Leaf Area

Plant cell death and *Hpa* structures were determined by staining leaves with lactophenol trypan blue (Alcázar et al., 2009). Samples were mounted on glycerol 70% and observed under light microscope (Axioplan; Carl Zeiss) coupled to a Leica DFC490 digital camera. Leaf area was quantified using Image Pro Analyzer (Media Cybernetics) as reported by Alcázar et al. (2009).

Isolation of *Hyaloperonospora arabidopsidis* Gw and Pathogen Inoculation Assays

Original spores from *H. arabidopsidis* Gw were collected from the Gw-16 accession naturally growing in the Gorzów population during spring of 2014. Spores were resuspended in 100 µL of water and inoculated on the susceptible Ws *eds1-1* genotype (Falk et al., 1999). Thereafter, the *Hpa* Gw isolate has been maintained by weekly propagation on the susceptible Gw-16 accession. *Hpa* inoculation assays were performed as described by Alcázar et al. (2009). *Pseudomonas syringae* spray inoculation and growth quantitation assays were performed as described by Alcázar et al. (2010).

Cloning of *ATR1*

The genomic DNA from *Hpa* Gw mass conidiospores was extracted using TriZol (Thermo Fisher) and used for PCR amplification of *ATR1* gene using primer combinations listed in Supplemental Table S11 (Rehmany et al., 2005). The PCR product was treated with ExoSap (Thermo Fisher) and sequenced by SANGER with primers described in Supplemental Table S11.

Global Metabolite Profiling

Metabolite profiling was performed from leaf samples (120 mg) using at least 10 biological replicates. Polar primary metabolite extraction and gas chromatography coupled to electron impact ionization-time of flight-mass spectrometry analysis was performed as described (Zarza et al., 2017). Only metabolites identified in all genotypes and at least 8 of 10 replicates were considered. Normalized values are referred to the internal standard. Principal component analysis was determined using *R* (www.r-project.org). HCA with Pearson correlation was obtained using the MultiExperiment Viewer software (http://mev.tm4.org/; version 27 4.8.1).

Starch Quantification

The entire shoot of 5-week-old plants was used for the analyses. Samples were harvested 1 h before the end of the light or dark periods. Starch levels were quantified according to Smith and Zeeman (2006) using at least five biological replicates per genotype.

Invertase Activities

Cell-wall-bound and soluble acid invertase activities were performed according to Appeldoorn et al. (1997) from leaves of 5-week-old Arabidopsis plants using at least five biological replicates per genotype.

Transient Expression Assays

Genomic versions of *RPP1-like* L*er R2*, *R3*, *R4*, and *R8* were obtained by PCR amplification from L*er* gDNA using the primers combinations listed in Supplemental Table S11. The PCR products were purified and cloned into the pSPARKII vector (Canvax). The resulting clones were sequenced using primers already described (Alcázar et al., 2014) and subcloned *Sal*I/*Not*I into a modified version of pENTR1A providing gentamycin resistance. The resulting construct was used for LR Gateway (Thermo Fisher) reaction with pEarley101 (Earley et al., 2006) to generate C terminus YFP-HA fusions of genomic clones under the control of the *Cauliflower mosaic virus* 35s promoter. The different constructs were sequenced, transformed into *A. tumefaciens* GV3101 pMP90, and used for infiltration of tobacco (*Nicotiana tabacum*; Samsun, SNN) leaves. Transformed agrobacteria were inoculated into 30 mL YEB media and incubated by shaking at 250 rpm and 28°C overnight. Cultures were centrifuged at 4,000*g* for 5 min and resuspended on 10 mM $MgCl_2$ and 10 mM MES, pH 5.6, to an OD_{600} of 0.45. For induction of agrobacteria virulence, 150 µM acetosyringone was added to the cells for 3 h. Discs from inoculated leaves were collected at indicated time points using a cork borer (1.2 cm diameter) and frozen immediately in liquid nitrogen. Pictures were taken at indicated time points with a Canon EOS 450D digital camera.

Western-Blot Analysis

Frozen samples were disrupted in 1.5-mL tubes along with 1-mm glass beads in a homogenizer device. Samples were suspended on 200 µL of protein extraction buffer (0.24 M Tris, pH 6.8, 6% SDS, 30% glycerol, 16% 2-mercaptoethanol, 0.01% bromophenol blue, and 10 M urea), boiled for 5 min, and centrifuged for 5 min at 12,000*g*. The supernatant was then transferred to a new tube. Fifteen microliters were used for 8% SDS-PAGE and transferred by blotting to a polyvinylidene difluoride membrane. Anti-GFP monoclonal antibody (clones 7.1 and 13.1; Roche) at 1:1,000 dilution and rabbit anti-mouse HRP (Sigma-Aldrich) secondary antibody at 1:10,000 were used for detection of YFP-tagged proteins with SuperSignal West Femto Maximum Sensitivity Chemiluminescent Substrate (Thermo Fisher).

QTL and GWAS Mapping

QTL mapping was performed using *R/qtl* with the genetic data of the L*er*/Sha RIL population from Clerkx et al. (2004) and phenotype evaluation of *Hpa* Gw disease resistance in Supplemental Table S6. For phenotypic evaluation, values from 0 to 2 were assigned to each genotype (0, no sporulation; 1, sporulation only observed on cotyledons; 2, sporulation observed in cotyledons and fully expanded leaves). LOD scores were calculated with a single-QTL model implemented in *R/qtl*. LOD score significance threshold was established using 1,000 permutations. GWAS mapping was performed using accessions and phenotypes listed in Supplemental Table S8. Manhattan plots were determined using 250 k SNP data and the accelerated mixed model (Kang et al., 2010; Zhang et al., 2010) implemented in GWAPP (Seren et al., 2012). To ensure adequate correction for population stratification, we constructed a *quantile-quantile* plot (Supplemental Fig. S14). A list of most significant associations is found in Supplemental Table S9.

Accession Numbers

RNA-seq data have been deposited to ArrayExpress (www.ebi.ac.uk/arrayexpress/) under accession number E-MTAB-6755.

Supplemental Data

The following supplemental materials are available.

Supplemental Figure S1. Leaf area and trypan blue staining in 5-week-old *sulki1*, *sulki2*, L*er*/Kas2 NIL, cNIL (Alcázar et al., 2010), and parental accessions grown at 14°C to 16°C.

Supplemental Figure S2. Alignment of amino acid sequences for *RPP1-like* genes in L*er*, Col-0, Uk-1, Bla-1, and Ws.

Supplemental Figure S3. RT-qPCR expression analyses of *PR1*, *RPP1-like* L*er R2*, *R3*, *R4*, and *R8* genes in L*er* plants treated with 100 µM benzo (1,2,3) thiadiazole-7-carbothioic acid *S*-methyl ester or 100 µM SA.

Supplemental Figure S4. CRISPR/Cas9-induced indel mutations in Cas9-*r2*, Cas9-*r3*, Cas9-*r4*, and Cas9-*r8* and their effects on protein translation.

Supplemental Figure S5. Leaf area and trypan blue staining of 5-week-old CRISPR/Cas9 *RPP1-like* L*er* mutants grown at 14°C to 16°C.

Supplemental Figure S6. Complementation of *sulki2-1* with *RPP1-like* L*er R3* gene reconstitutes L*er*/Kas2 NIL phenotype.

Supplemental Figure S7. *PR1*, *EDS1*, and *GST1* expression analyses in 5- and 7-week-old (w-o) Cas9 *r2-1*, *r2-2*, *r3-1*, *r3-2*, *r4-1*, *r4-2*, *r8-1*, and *r8-2*, L*er*, Kas2, L*er*/Kas2 NIL, and cNIL plants grown at 14°C to 16°C.

Supplemental Figure S8. Starch levels determined in leaves of 5-week-old incompatible L*er*/Kas2 NIL, Kas2, L*er*, *sulki1-1*, *sulki1-7*, *sulki1-8*, and *sulki1-9* grown at 14°C to 16°C.

Supplemental Figure S9. Apoplastic and vacuolar invertase activities of 5-week-old incompatible L*er*/Kas2 NIL, Kas2, L*er*, *sulki1-1*, *sulki1-7*, *sulki1-8*, and *sulki1-9* grown at 14°C to 16°C.

Supplemental Figure S10. Neighbor-joining phylogenetic analysis of ATR1 amino acid sequences from different *Hpa* isolates.

Supplemental Figure S11. Disease resistance phenotypes to *Hpa* Gw infection in different genotypes.

Supplemental Figure S12. Principal component analysis of the Gw population based on 134 genome-wide SNPs.

Supplemental Figure S13. Coverage of Illumina reads mapping to the *At3g44400-At3g44480* interval in L*er*.

Supplemental Figure S14. Quantile-quantile (Q-Q) plot for GWAS analysis of *Hpa* Gw disease resistance using the accelerated mixed model method.

Supplemental Table S1. Segregation analyses of *sulki* and CRISPR/Cas9 mutants.

Supplemental Table S2. List of differentially expressed genes in the comparisons between Kas2 versus L*er*/Kas2 NIL and *sulki1-8* versus L*er*/Kas2 NIL and their Gene Ontology analyses.

Supplemental Table S3. List of metabolites and raw data from GC/MS analyses in L*er*/Kas2 NIL, Kas2, L*er*, *sulki1-1*, *sulki1-7*, *sulki1-8*, and *sulki1-9*.

Supplemental Table S4. PC1 and PC2 loadings of L*er*/Kas2 NIL, L*er*, Kas2, and *sulki1* metabolite profiles.

Supplemental Table S5. Genotype data and disease resistance phenotypes to *Hpa* Gw infection in the Gorzów population.

Supplemental Table S6. Phenotype data for disease resistance to *Hpa* Gw in the L*er*/Sha RIL population.

Supplemental Table S7. List of *NLR* genes in the QTL interval of chromosome one for *Hpa* Gw disease resistance in the L*er*/Sha RIL population.

Supplemental Table S8. List of accessions used in GWAS mapping for disease resistance to *Hpa* Gw infection.

Supplemental Table S9. List of genes with highest associations in GWAS mapping for disease resistance to *Hpa* Gw.

Supplemental Table S10. Summary statistics of whole-genome sequencing and RNA-seq reads.

Supplemental Table S11. List of oligonucleotides used in this work.

ACKNOWLEDGMENTS

We thank Maarten Koornneef for biological materials and critical reading of the manuscript. We acknowledge support from the CNAG (Spain) in next-generation sequencing experiments.

Received April 18, 2018; accepted May 15, 2018; published May 23, 2018.

LITERATURE CITED

Aarts N, Metz M, Holub E, Staskawicz BJ, Daniels MJ, Parker JE (1998) Different requirements for EDS1 and NDR1 by disease resistance genes define at least two *R* gene-mediated signaling pathways in *Arabidopsis*. Proc Natl Acad Sci USA **95**: 10306–10311

Alcázar R, García AV, Parker JE, Reymond M (2009) Incremental steps toward incompatibility revealed by *Arabidopsis* epistatic interactions modulating salicylic acid pathway activation. Proc Natl Acad Sci USA **106**: 334–339

Alcázar R, García AV, Kronholm I, de Meaux J, Koornneef M, Parker JE, Reymond M (2010) Natural variation at *Strubbelig Receptor Kinase 3* drives immune-triggered incompatibilities between *Arabidopsis thaliana* accessions. Nat Genet **42**: 1135–1139

Alcázar R, Pecinka A, Aarts MGM, Fransz PF, Koornneef M (2012) Signals of speciation within *Arabidopsis thaliana* in comparison with its relatives. Curr Opin Plant Biol **15**: 205–211

Alcázar R, von Reth M, Bautor J, Chae E, Weigel D, Koornneef M, Parker JE (2014) Analysis of a plant complex *resistance* gene locus underlying immune-related hybrid incompatibility and its occurrence in nature. PLoS Genet **10**: e1004848

Appeldoorn NJG, de Bruijn SM, Koot-Gronsveld EAM, Visser RGF, Vreugdenhil D, van der Plas LHW (1997) Developmental changes of enzymes involved in conversion of sucrose to hexose-phosphate during early tuberisation of potato. Planta **202**: 220–226

Ariga H, Katori T, Tsuchimatsu T, Hirase T, Tajima Y, Parker JE, Alcázar R, Koornneef M, Hoekenga O, Lipka AE, (2017) NLR locus-mediated trade-off between abiotic and biotic stress adaptation in *Arabidopsis*. Nat Plants **3**: 17072

Bakker EG, Toomajian C, Kreitman M, Bergelson J (2006) A genome-wide survey of *R* gene polymorphisms in *Arabidopsis*. Plant Cell **18**: 1803–1818

Bartsch M, Gobbato E, Bednarek P, Debey S, Schultze JL, Bautor J, Parker JE (2006) Salicylic acid-independent ENHANCED DISEASE SUSCEPTIBILITY1 signaling in *Arabidopsis* immunity and cell death is regulated by the monooxygenase FMO1 and the Nudix hydrolase NUDT7. Plant Cell **18**: 1038–1051

Bernoux M, Ve T, Williams S, Warren C, Hatters D, Valkov E, Zhang X, Ellis JG, Kobe B, Dodds PN (2011) Structural and functional analysis of a plant resistance protein TIR domain reveals interfaces for self-association, signaling, and autoregulation. Cell Host Microbe **9**: 200–211

Bolton MD (2009) Primary metabolism and plant defense--fuel for the fire. Mol Plant Microbe Interact **22**: 487–497

Bomblies K (2010) Doomed lovers: mechanisms of isolation and incompatibility in plants. Annu Rev Plant Biol **61**: 109–124

Bomblies K, Weigel D (2007) Hybrid necrosis: autoimmunity as a potential gene-flow barrier in plant species. Nat Rev Genet **8**: 382–393

Bomblies K, Lempe J, Epple P, Warthmann N, Lanz C, Dangl JL, Weigel D (2007) Autoimmune response as a mechanism for a Dobzhansky-Muller-type incompatibility syndrome in plants. PLoS Biol **5**: e236

Botella MA, Parker JE, Frost LN, Bittner-Eddy PD, Beynon JL, Daniels MJ, Holub EB, Jones JD (1998) Three genes of the *Arabidopsis RPP1* complex resistance locus recognize distinct *Peronospora parasitica* avirulence determinants. Plant Cell **10**: 1847–1860

Bowling SA, Guo A, Cao H, Gordon AS, Klessig DF, Dong X (1994) A mutation in *Arabidopsis* that leads to constitutive expression of systemic acquired resistance. Plant Cell **6**: 1845–1857

Cao J, Schneeberger K, Ossowski S, Günther T, Bender S, Fitz J, Koenig D, Lanz C, Stegle O, Lippert C, (2011) Whole-genome sequencing of multiple *Arabidopsis thaliana* populations. Nat Genet **43**: 956–963

Chae E, Bomblies K, Kim S-TT, Karelina D, Zaidem M, Ossowski S, Martín-Pizarro C, Laitinen RAE AE, Rowan BAA, Tenenboim H, (2014)Species-wide

genetic incompatibility analysis identifies immune genes as hot spots of deleterious epistasis. Cell **159**: 1341–1351

Chen C, Chen H, Lin Y-S, Shen J-B, Shan J-X, Qi P, Shi M, Zhu M-Z, Huang X-H, Feng Q, (2014) A two-locus interaction causes interspecific hybrid weakness in rice. Nat Commun **5**: 3357

Clerkx EJM, El-Lithy ME, Vierling E, Ruys GJ, Blankestijn-De Vries H, Groot SPC, Vreugdenhil D, Koornneef M (2004) Analysis of natural allelic variation of Arabidopsis seed germination and seed longevity traits between the accessions Landsberg *erecta* and Shakdara, using a new recombinant inbred line population. Plant Physiol **135**: 432–443

Coates ME, Beynon JL (2010) *Hyaloperonospora Arabidopsidis* as a pathogen model. Annu Rev Phytopathol **48**: 329–345

Coyne JA (1992) Genetics and speciation. Nature **355**: 511–515

Coyne JA, Orr HA (2004) Speciation. Sinauer Associates, Sunderland, MA

Dettman JR, Sirjusingh C, Kohn LM, Anderson JB (2007) Incipient speciation by divergent adaptation and antagonistic epistasis in yeast. Nature **447**: 585–588

Dodds PN, Rathjen JP (2010) Plant immunity: towards an integrated view of plant-pathogen interactions. Nat Rev Genet **11**: 539–548

Doyle J (1991) DNA protocols for plants. *In* **GM Hewitt, AWB Johnston, JPW Young**, eds, Molecular Techniques in Taxonomy, Springer, Berlin, pp 283–293

Earley KW, Haag JR, Pontes O, Opper K, Juehne T, Song K, Pikaard CS (2006) Gateway-compatible vectors for plant functional genomics and proteomics. Plant J **45**: 616–629

Falk A, Feys BJ, Frost LN, Jones JD, Daniels MJ, Parker JE (1999) EDS1, an essential component of R gene-mediated disease resistance in *Arabidopsis* has homology to eukaryotic lipases. Proc Natl Acad Sci USA **96**: 3292–3297

Fauser F, Schiml S, Puchta H (2014) Both CRISPR/Cas-based nucleases and nickases can be used efficiently for genome engineering in *Arabidopsis thaliana*. Plant J **79**: 348–359

Feys BJ, Moisan LJ, Newman MA, Parker JE (2001) Direct interaction between the *Arabidopsis* disease resistance signaling proteins, EDS1 and PAD4. EMBO J **20**: 5400–5411

Feys BJ, Wiermer M, Bhat RA, Moisan LJ, Medina-Escobar N, Neu C, Cabral A, Parker JE (2005) Arabidopsis SENESCENCE-ASSOCIATED GENE101 stabilizes and signals within an ENHANCED DISEASE SUSCEPTIBILITY1 complex in plant innate immunity. Plant Cell **17**: 2601–2613

Flynn KM, Cooper TF, Moore FB-G, Cooper VS (2013) The environment affects epistatic interactions to alter the topology of an empirical fitness landscape. PLoS Genet **9**: e1003426

Goritschnig S, Steinbrenner AD, Grunwald DJ, Staskawicz BJ (2016) Structurally distinct *Arabidopsis thaliana* NLR immune receptors recognize tandem WY domains of an oomycete effector. New Phytol **210**: 984–996

Hurwitz BL, Kudrna D, Yu Y, Sebastian A, Zuccolo A, Jackson SA, Ware D, Wing RA, Stein L (2010) Rice structural variation: a comparative analysis of structural variation between rice and three of its closest relatives in the genus Oryza. Plant J **63**: 990–1003

Jeuken MJW, Zhang NW, McHale LK, Pelgrom K, den Boer E, Lindhout P, Michelmore RW, Visser RGF, Niks RE (2009) Rin4 causes hybrid necrosis and race-specific resistance in an interspecific lettuce hybrid. Plant Cell **21**: 3368–3378

Kang HM, Sul JH, Service SK, Zaitlen NA, Kong SY, Freimer NB, Sabatti C, Eskin E (2010) Variance component model to account for sample structure in genome-wide association studies. Nat Genet **42**: 348–354

Khan M, Subramaniam R, Desveaux D (2016) Of guards, decoys, baits and traps: pathogen perception in plants by type III effector sensors. Curr Opin Microbiol **29**: 49–55

Kopka J, Schauer N, Krueger S, Birkemeyer C, Usadel B, Bergmüller E, Dörmann P, Weckwerth W, Gibon Y, Stitt M, (2005) GMD@CSB.DB: the Golm Metabolome Database. Bioinformatics **21**: 1635–1638

Krasileva KV, Dahlbeck D, Staskawicz BJ (2010) Activation of an *Arabidopsis* resistance protein is specified by the in planta association of its leucine-rich repeat domain with the cognate oomycete effector. Plant Cell **22**: 2444–2458

Krüger J, Thomas CM, Golstein C, Dixon MS, Smoker M, Tang S, Mulder L, Jones JDG (2002) A tomato cysteine protease required for Cf-2-dependent disease resistance and suppression of autonecrosis. Science **296**: 744–747

McDowell JM, Cuzick A, Can C, Beynon J, Dangl JL, Holub EB (2000) Downy mildew (*Peronospora parasitica*) resistance genes in *Arabidopsis* vary in functional requirements for NDR1, EDS1, NPR1 and salicylic acid accumulation. Plant J **22**: 523–529

McHale LK, Haun WJ, Xu WW, Bhaskar PB, Anderson JE, Hyten DL, Gerhardt DJ, Jeddeloh JA, Stupar RM (2012) Structural variants in the soybean genome localize to clusters of biotic stress-response genes. Plant Physiol **159**: 1295–1308

Meyers BC, Kozik A, Griego A, Kuang H, Michelmore RW (2003) Genome-wide analysis of NBS-LRR-encoding genes in *Arabidopsis*. Plant Cell **15**: 809–834

Muñoz-Amatriaín M, Eichten SR, Wicker T, Richmond TA, Mascher M, Steuernagel B, Scholz U, Ariyadasa R, Spannagl M, Nussbaumer T, (2013) Distribution, functional impact, and origin mechanisms of copy number variation in the barley genome. Genome Biol **14**: R58

Ono J, Gerstein AC, Otto SP (2017) Widespread genetic incompatibilities between first-step mutations during parallel adaptation of *Saccharomyces cerevisiae* to a common environment. PLoS Biol **15**: e1002591

Rehmany AP, Gordon A, Rose LE, Allen RL, Armstrong MR, Whisson SC, Kamoun S, Tyler BM, Birch PRJ, Beynon JL (2005) Differential recognition of highly divergent downy mildew avirulence gene alleles by *RPP1* resistance genes from two *Arabidopsis* lines. Plant Cell **17**: 1839–1850

Schreiber KJ, Bentham A, Williams SJ, Kobe B, Staskawicz BJ (2016) Multiple domain associations within the *Arabidopsis* immune receptor RPP1 regulate the activation of programmed cell death. PLoS Pathog **12**: e1005769

Seren Ü, Vilhjálmsson BJ, Horton MW, Meng D, Forai P, Huang YS, Long Q, Segura V, Nordborg M (2012) GWAPP: a web application for genome-wide association mapping in *Arabidopsis*. Plant Cell **24**: 4793–4805

Sherlock G, Petrov DA (2017) Seeking goldilocks during evolution of drug resistance. PLoS Biol **15**: e2001872

Sicard A, Kappel C, Josephs EB, Lee YW, Marona C, Stinchcombe JR, Wright SI, Lenhard M (2015) Divergent sorting of a balanced ancestral polymorphism underlies the establishment of gene-flow barriers in Capsella. Nat Commun **6**: 7960

Smith AM, Zeeman SC (2006) Quantification of starch in plant tissues. Nat Protoc **1**: 1342–1345

Sohn KH, Lei R, Nemri A, Jones JDG (2007) The downy mildew effector proteins ATR1 and ATR13 promote disease susceptibility in *Arabidopsis thaliana*. Plant Cell **19**: 4077–4090

Steinbrenner AD, Goritschnig S, Staskawicz BJ (2015) Recognition and activation domains contribute to allele-specific responses of an Arabidopsis NLR receptor to an oomycete effector protein. PLoS Pathog **11**: e1004665

Stuttmann J, Peine N, Garcia AV, Wagner C, Choudhury SR, Wang Y, James GV, Griebel T, Alcázar R, Tsuda K, (2016) *Arabidopsis thaliana* DM2h (R8) within the Landsberg *RPP1-like* resistance locus underlies three different cases of EDS1-conditioned autoimmunity. PLoS Genet **12**: e1005990

Sukarta OCA, Slootweg EJ, Goverse A (2016) Structure-informed insights for NLR functioning in plant immunity. Semin Cell Dev Biol **56**: 134–149

Swiderski MR, Birker D, Jones JDG (2009) The TIR domain of TIR-NB-LRR resistance proteins is a signaling domain involved in cell death induction. Mol Plant Microbe Interact **22**: 157–165

Takken FLW, Goverse A (2012) How to build a pathogen detector: structural basis of NB-LRR function. Curr Opin Plant Biol **15**: 375–384

Tauzin AS, Giardina T (2014) Sucrose and invertases, a part of the plant defense response to the biotic stresses. Front Plant Sci **5**: 293

van Ooijen G, Mayr G, Kasiem MM, Albrecht M, Cornelissen BJ, Takken FL (2008) Structure-function analysis of the NB-ARC domain of plant disease resistance proteins. J Exp Bot **59**: 1383–1397

Wildermuth MC, Dewdney J, Wu G, Ausubel FM (2001) Isochorismate synthase is required to synthesize salicylic acid for plant defence. Nature **414**: 562–565

Williams SJ, Sohn KH, Wan L, Bernoux M, Sarris PF, Segonzac C, Ve T, Ma Y, Saucet SB, Ericsson DJ, (2014) Structural basis for assembly and function of a heterodimeric plant immune receptor. Science **344**: 299–303

Xu X, Liu X, Ge S, Jensen JD, Hu F, Li X, Dong Y, Gutenkunst RN, Fang L, Huang L, (2011) Resequencing 50 accessions of cultivated and wild rice yields markers for identifying agronomically important genes. Nat Biotechnol **30**: 105–111

Yamamoto E, Takashi T, Morinaka Y, Lin S, Wu J, Matsumoto T, Kitano H, Matsuoka M, Ashikari M (2010) Gain of deleterious function causes an autoimmune response and Bateson-Dobzhansky-Muller incompatibility in rice. Mol Genet Genomics **283**: 305–315

Yuan J, He SY (1996) The *Pseudomonas syringae* Hrp regulation and secretion system controls the production and secretion of multiple extracellular proteins. J Bacteriol **178**: 6399–6402

Zarza X, Atanasov KE, Marco F, Arbona V, Carrasco P, Kopka J, Fotopoulos V, Munnik T, Gómez-Cadenas A, Tiburcio AF, (2017) *Polyamine oxidase 5* loss-of-function mutations in *Arabidopsis thaliana* trigger metabolic and transcriptional reprogramming and promote salt stress tolerance. Plant Cell Environ **40**: 527–542

Zhang X, Bernoux M, Bentham AR, Newman TE, Ve T, Casey LW, Raaymakers TM, Hu J, Croll TI, Schreiber KJ, (2017) Multiple functional self-association interfaces in plant TIR domains. Proc Natl Acad Sci USA **114**: E2046–E2052

Zhang Z, Ersoz E, Lai C-Q, Todhunter RJ, Tiwari HK, Gore MA, Bradbury PJ, Yu J, Arnett DK, Ordovas JM, (2010) Mixed linear model approach adapted for genome-wide association studies. Nat Genet **42**: 355–360